

## The Surface Chemistry of Almandine Garnet

*Jeffrey Poon<sup>1</sup>, David C. Madden<sup>1</sup>, Mary H. Wood<sup>1#</sup>, Ron van Tol<sup>2</sup>, Hans Sonke<sup>2</sup>, and Stuart M.*

*Clarke<sup>\*1</sup>*

<sup>1</sup> BP Institute and Department of Chemistry, University of Cambridge, Cambridge UK, CB3 0EZ

<sup>2</sup> Shell Global Research Centre, Amsterdam, The Netherlands

# Present address: School of Chemistry, University of Birmingham, Birmingham, B15 2TT

\* Corresponding author: [stuart@bpi.cam.ac.uk](mailto:stuart@bpi.cam.ac.uk); +00 44 (0) 1223 765700

### **Abstract**

Almandine garnet is commonly used in abrasive blasting processes to prepare metallic surfaces for painting. However, there is evidence that the process leads to significant amounts of abrasive embedded in the 'cleaned' surface, and hence the surface chemistry of garnet will affect the binding of any coatings subsequently applied. In addition, in marine environments seawater aerosol droplets are expected to impact the exposed surface prior to coating application, depositing both water and dissolved inorganic ions. In this work, we provide in-depth analysis of the chemistry of the almandine garnet surface using angle-resolved X-ray photoelectron spectroscopy (XPS) and note a correlation for several elemental oxides between literature values of the binding energy of the surface oxygen 1s XPS peak and the basicity of the hydroxyl group that forms on the surface. We also consider the adsorption to almandine garnet powder of seawater-relevant inorganic ions (sodium, magnesium, and calcium): Binding constants have been determined using titration measurements, solution-depletion isotherms, and numerical modelling, with calcium observed to bind more strongly than magnesium. The relevance of Langmuir-type fits to constant-pH adsorption isotherms is discussed. By contrast, sodium either binds very weakly or is effectively inert towards

the garnet surface under the experimental conditions. The complex adsorption behaviour observed emphasizes the necessity of using multiple techniques to characterize mineral surfaces.

## Introduction

Garnets are a group of silicate minerals, that have the general formula  $X_3Y_2(SiO_4)_3$ . The X sites are usually occupied by divalent cations (*e.g.* Ca, Mg, Fe, Mn, *etc.*) whilst the Y sites are often occupied by trivalent cations (*e.g.* Al, Fe, Cr, *etc.*) coordinated by six oxygen atoms to form octahedra. An octahedral-tetrahedral crystal framework is thus formed, with  $SiO_4^{2-}$  units forming the tetrahedra.<sup>1</sup> Almandine garnet, where X is Fe and Y is Al, (*i.e.*  $Fe_3Al_2(SiO_4)_3$ ) is illustrated in Figure S1 in the Supporting Information. As they are hard, readily available, and inexpensive compared to alternatives such as silicon carbide and diamond, natural garnet minerals are widely used in manufacturing and engineering processes as abrasives for surface grinding, abrasive blasting, and water-jet cutting.<sup>2,3</sup> In 2004, world garnet production was over 280,000 tonnes (mainly mined in Australia and India). For abrasive applications, almandine garnet is deemed superior to other garnets due to its greater hardness.<sup>4</sup>

Despite the many industrial and research applications of garnet minerals, there have been few papers addressing their surface chemistry and the adsorption of species onto their surfaces. There has been recent work addressing adsorption from non-aqueous solvents and the comparison with metal substrates,<sup>5</sup> and it is known that almandine garnet has no preferred cleavage plane.<sup>6,7</sup> There has been some work by Jia and Sun on almandine garnet's flotation characteristics and the adsorption of inorganic ions,<sup>8,9</sup> in which experimental data is rationalised using the surface groups that may be predicted based on the bulk crystal structure and surface charge effects. It was speculated that the surface groups are  $\{AlO_6\}$  octahedra, as observed in the bulk crystal, with the adsorbate ion being doubly coordinated to two oxygens linked to the aluminium cation. However, these assertions have not been verified with characterisation of the mineral using surface-sensitive techniques.

It is well known that garnet-blasted surfaces often have significant amounts of abrasive residue embedded.<sup>5</sup> This emphasizes that the surface chemistry of the mineral could affect the performance of abrasive-blasted materials, such as carbon steel, and any coatings subsequently applied. In marine environments, abrasive-blasted surfaces may be exposed for extended periods prior to the application of protective coatings; in this time, aerosol droplets that impact the surface can initiate corrosion and deposit inorganic ions.<sup>10</sup> Therefore, any change to garnet surfaces when exposed to these ions may affect the adhesion of coatings subsequently applied.

The lack of a preferred cleavage plane for garnet makes it likely that the surfaces formed when the bulk mineral fractures (for example, when garnet is mined for use as an abrasive) are rather heterogeneous, with multiple different surface planes and terminations exposed. This heterogeneity is expected to increase on exposure to an aqueous environment, due to the formation of surface hydroxyl groups,<sup>11</sup> reaction with dissolved ions,<sup>9,12</sup> and the possibility of dissolution and reprecipitation processes occurring.<sup>13</sup> These complex surfaces are the focus of this work. One possible termination of the almandine {110} surface (on exposure to an aqueous environment) is illustrated schematically in Figure 1, highlighting the complexity of the situation, even when only a single termination of one surface plane is considered.

In this work, we extend the characterisation of almandine garnet using X-ray photoelectron spectroscopy (XPS), which indicates the elements present at the surface and their chemical environments, allowing the thickness and constituents of the surface layer to be inferred. We also present data from a range of experimental techniques, complemented by numerical modelling, on the behaviour of almandine garnet when exposed to aqueous solution: these provide values for the number density of surface sites present, their intrinsic acidities and basicities, and the strength of binding of seawater-relevant inorganic ions. The numbers obtained will be compared, in the

context of the limitations of the different methods; the range of values highlights the importance of employing a multi-technique approach, such as this, to obtain a comprehensive understanding of the surface chemistry of a mineral.

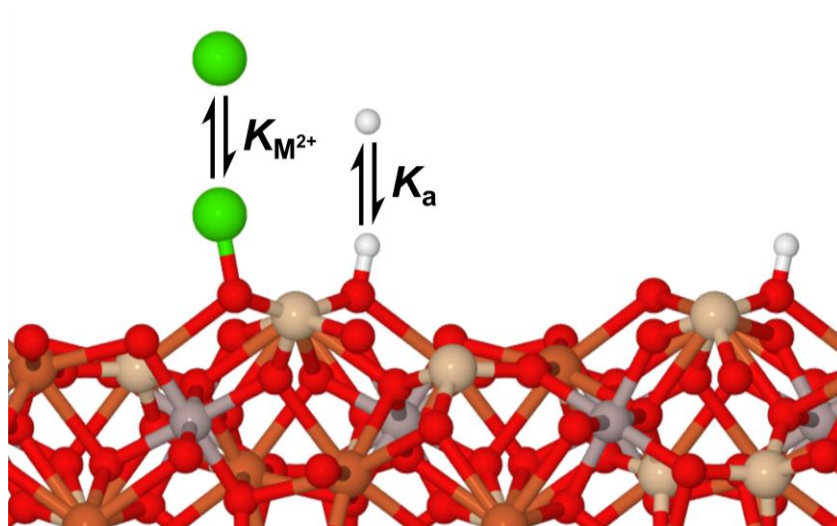


**Figure 1:** A schematic illustration of one bulk termination of the almandine garnet {110} surface, on exposure to an aqueous environment. Fe, Al, Si, O, and H atoms are shown in brown, grey, cream, red, and white respectively. In this work, we aim to quantify the thickness and constituents of the surface layer, the number density of surface hydroxyl groups, their acidities and basicities ( $K_a$  values), and the strength of binding of aqueous  $Mg^{2+}$  and  $Ca^{2+}$  ions (shown in green).

## Methods

### Chemicals and Reagents

All reagents used were supplied by Sigma-Aldrich Company Ltd., Gillingham, UK, unless otherwise stated. 69 %/wt nitric acid was supplied by VWR, Lutterworth, UK. All aqueous solutions and suspensions were made up using ultrapure water with resistivity of 18.2 M $\Omega$  cm.

### XPS

A piece of almandine garnet was cut arbitrarily, then the flat surface was polished using increasingly fine diamond paste (from Kemet, Kent, UK: 25  $\mu\text{m}$ , 14  $\mu\text{m}$ , 6  $\mu\text{m}$ , 1  $\mu\text{m}$ , and 100 nm). The polished substrate was washed in 2 %/wt Decon90<sup>®</sup> solution (Decon Laboratories Limited), sonicated for 1 minute, and then soaked in 2 %/wt Decon90 overnight. The sample was then rinsed ten times with 50 mL of ultrapure water, sonicated in ultrapure water for 1 minute, soaked in ultrapure water overnight, and rinsed with ultrapure water ten times to remove any excess detergent. Finally, the surface was dried with a jet of dry nitrogen. The washing procedure was intended to remove all diamond paste residues (and Decon90<sup>®</sup> surfactant), thereby ensuring that the polished surface resembles a fractured garnet surface that has been exposed to an aqueous environment. This preparation method was used to ensure that the flat surface and the powdered samples described subsequently are as comparable as possible, with both being relevant to the surfaces of garnet abrasives used in marine environments.

Angle-resolved XPS (AR-XPS), in which the detector is tilted at an angle,  $\vartheta$ , with respect to the surface normal, was employed to increase the surface sensitivity of the measurements: the larger the tilt angle, the greater the contribution to the measured signal from the surface region, due to the short inelastic mean free path of electrons excited in the solid by the X-ray beam.

Preliminary XPS data were taken with an ESCALAB 250Xi spectrometer (Thermo Fisher Scientific, Hillsboro, USA) with a monochromated Al K-alpha source (1486.68 eV) at the Cavendish Laboratory, University of Cambridge. XP spectra were also obtained with a monochromatic 1486.68 eV source, using a Thermo Theta Probe Mk III spectrometer system at University College London (part of the Harwell XPS service). In both of the instruments, the angle was varied at 5° increments: the ESCALAB 250Xi was used to study tilt angles between 0 and 50°; in the Thermo Theta system, the range was 22.5 to 77.5°. Energy steps of 0.1 eV were used, and the diameter of the X-ray beam was

400  $\mu\text{m}$ . Two spots were examined for each of the two samples prepared; the data for the two spots showed only minor differences.

Charge compensation was provided by a dual-mode (argon ion and electron) flood gun. The analyser was operated in constant analyser energy (CAE) mode, with a pass energy of 50 eV. The total acquisition time for each core line was approximately 50 minutes. Survey spectra were collected as above, except that the pass energy was 200 eV and parallel angle resolved data were not collected. The total time to collect a survey spectrum was approximately 5 minutes.

Detailed spectral analysis was conducted using CasaXPS software, with the alkyl carbon peak (C-C) at 284.8 eV binding energy as a reference, to deconvolute the components contributing to peaks. All fittings use 70% Gaussian and 30% Lorentzian peaks (GL(30) setting); the backgrounds used were generated with the Shirley method.<sup>14,15</sup> The variation of peak areas with increasing surveying angle allowed for the discrimination of surface and bulk components. The thickness of the surface layer was then estimated using data for each of the elements (assuming a constant inelastic mean free path of the excited electrons and a surface that maintains an ideal, bulk-terminated structure); the method will be described in more detail subsequently.

### **Almandine Garnet Powder**

Almandine garnet powder was supplied by GMA Garnet, Geraldton, Australia. As a natural mineral, this contains other trace minerals. A summary of the quoted composition is shown in Table S1 in the Supporting Information. To maximise the surface-to-mass ratio of the garnet, the solids were milled in 60 g batches using a PM100 planetary ball mill, Retsch GmbH, Hann, Germany, in a 125 mL tungsten carbide jar, with seven 20 mm tungsten carbide milling balls. Each batch was milled at 500 rpm for 20 minutes in total. The milling direction was changed at ten-minute intervals.

To minimise other impurity species in the natural garnet mineral contributing extra inorganic ions in aqueous adsorption experiments, a washing procedure, which has been described in detail previously,<sup>5</sup> was employed. In summary, the milled garnet was washed with 30 mL 10 %/wt nitric acid, then six times with 30 mL ultrapure water, before being dried in vacuum (at 100 °C for six hours). As will be discussed subsequently, although the washed garnet is observed to dissolve at very low pH, no significant amount of calcium ions is released into the aqueous solution, confirming that the washing process is effective in removing calcium carbonate impurities from the powder.<sup>5</sup> The specific surface area of the acid-washed garnet powder was found through Brunauer–Emmett–Teller (BET) isotherm to be 5.54 ( $\pm$  0.03) m<sup>2</sup> g<sup>-1</sup> (using a TriStar 3000, Micromeritics, at the Department of Materials and Metallurgy, University of Cambridge).

Powder X-ray diffraction (PXRD) analyses were performed at room temperature using a Panalytical X'Pert Pro diffractometer with Ni-filtered Cu-K $\alpha$  radiation (wavelength, 1.5418 Å) equipped with an RTMS X'celerator detector, at the Department of Chemistry, University of Cambridge. For each measurement, a sample of the powder was ground, then gently pressed on a recessed glass disc to give a flat surface and subsequently analysed. The data were collected in the 2 $\theta$  range of 5–90° using a step size of 0.0167° and a scan speed of 0.02° s<sup>-1</sup>; during data collection the sample was rotated. For each analysis, the total number of steps was 5086 and the total time was 72 minutes.

PXRD data were obtained before and after the acid washing procedure, and after tumbling the garnet powders for one week in ultrapure water, or 0.1 M hydrochloric acid or sodium hydroxide. All patterns matched the characteristic almandine garnet spectrum with no evidence of other ordered phases present, as shown in Figure S2 in the Supporting Information, confirming that neither the acid washing procedure nor the exposure of the acid-washed garnet powder to strong

acid or base (for durations longer than those of the titration, adsorption isotherm, and  $\zeta$ -potential measurements described subsequently) significantly changes the nature of the bulk garnet powder.

### **Garnet Dissolution Studies**

2.0 g acid-washed garnet was placed into 50 mL polypropylene centrifuge tubes (Falcon® Brand, Corning Inc., USA), with 10 mL 9 mM nitric acid in 100 mM sodium nitrate, for varying times. The samples were then centrifuged for 30 minutes under a centrifugal force of 15000 g, using a Heraeus Multifuge 1 S-R, by Thermo Scientific, Waltham, USA. The supernatant was carefully withdrawn using a pipette; half was acidified to 1 %/wt nitric acid using 69 %/wt nitric acid and analysed using Inductive coupled plasma optical emission spectrometry (ICP-OES), with a PerkinElmer Optima 8000 ICP-OES Spectrometer, at the Department of Geography, University of Cambridge to detect calcium and aluminium in solution, from which the masses of almandine garnet ( $\text{Fe}_3\text{Al}_2(\text{SiO}_4)_3$ ) and calcium carbonate ( $\text{CaCO}_3$ ) that had dissolved were calculated. The other half of the supernatant was used for pH measurement with a Unitrode Pt100 pH probe attached to a Metrohm 809 Titrando, Metrohm UK Ltd., Runcorn, UK, at the BP Institute, University of Cambridge.

To further understand the dissolution behaviour of the acid-washed garnet powder, ICP-OES measurements of iron, aluminium, and silicon were taken from the supernatants obtained from the tumbled samples in ultrapure water, or 0.1 M hydrochloric acid or sodium hydroxide, the solids from which were used for PXRD analysis (as described in the previous section). These ICP-OES data were obtained with a Thermo Scientific Ltd. iCAP Duo at the Department of Chemistry. Standard ranges were prepared by diluting certified 1000 mg L<sup>-1</sup> stock calibrants (Si Standard for AAS, Sigma Aldrich, and Multi-Element Calibration Standard for IV for ICP, VWR Chemicals) into 2 %/wt nitric acid. For silicon standards, plastic containers were used throughout. Where required, samples were

diluted in ultrapure water. The measurements were made in axial mode at emission wavelengths of 238.204, 396.152, and 251.611 nm for iron, aluminium, and silicon respectively.

### **Salt-Solution Titrations, Acid-Base Titrations and $\zeta$ -Potential Measurements**

The Metrohm 809 Titrando was used for salt-solution titrations and acid-base pH titrations. For the former, 10  $\mu\text{L}$  aliquots of 100 mM solutions of sodium, magnesium, or calcium nitrate were added to suspensions of 5 g acid-washed almandine garnet powder in 50 ml of ultrapure water (a concentration of 100 g  $\text{L}^{-1}$ ); for the latter, 10  $\mu\text{L}$  aliquots of 100 mM solutions of either sodium hydroxide or hydrochloric acid were added to suspensions of acid-washed almandine garnet in sodium nitrate solution. In both cases, the pH change of the solution was monitored.  $\zeta$ -Potential measurements were acquired using a Brookhaven Instruments ZetaPlus Zeta Potential Analyser, at the BP Institute. Suspension concentrations of 1 g  $\text{L}^{-1}$  were used, and solutions were contained in a clear plastic cuvette with 10 mm optical length. The suspension pH of each sample was measured using narrow-range pH indicator strips (with increments of 0.2 or 0.3 pH units) from Sigma-Aldrich. The errors quoted in the derived values were calculated from the variation of repeated measurements.

### **Adsorption Isotherm Sample Preparation**

Typically, 2.0 g acid-washed garnet was placed into 50 mL centrifuge tubes. Each sample was made up to a concentration of 200 g  $\text{L}^{-1}$ , with the appropriate amount of adsorbate solution (for variable-pH adsorption experiments, 0.5 mM magnesium nitrate, calcium nitrate, or sodium sulphate; for constant-pH adsorption experiments, varying concentrations of magnesium nitrate or calcium nitrate) in 100 mM sodium nitrate. 100 mM sodium hydroxide or nitric acid in 100 mM sodium nitrate was added to adjust the pH. The samples were tumbled to equilibrate for 24 hours at 20 °C, and then centrifuged for 30 minutes under a centrifugal force of 15000g. Half of the supernatant

was carefully removed with a pipette and analysed using ICP-OES to determine the equilibrated adsorbate concentration. The other half of the centrifuged samples was separated from the solids, and the equilibrium pH was tested using a pH probe.

## **Numerical Modelling**

All numerical calculations of the surface speciation and ion binding were performed using Visual MINTEQ, written by Jon Petter Gustafsson, Division of Land and Water Resources Engineering, KTH Royal Institute of Technology, Stockholm, Sweden. The standard thermodynamic database of MINTEQ, which was used without modification, contains relevant equilibria involving species in aqueous solution, and hence allows the behaviour at different pH to be predicted. Modelling of the adsorption of ions from aqueous solution to the garnet surface using a simple two-layer model was performed by including additional equilibria, representing the behaviour of the surface groups present and complexation of ions to these. The numbers of surface groups, the precise nature of the equilibria, and the equilibrium constants were chosen to best fit the different experimental data, as will be described subsequently. The goodness of fit of different models (for example, different adsorption equilibria) to experimental data was quantified by calculating the root-mean-square error in the different cases.

## **Results and Discussion**

### **X-Ray Photoelectron Spectroscopy**

To characterise the dry garnet surface, Angle-resolved X-ray photoelectron spectroscopy (XPS) data were collected from a polished almandine garnet crystal. Figure 2 shows the a) aluminium 2p, b) silicon 2p, and c) oxygen 1s regions at different surveying angles. When the detector is 22.5° from the surface normal, the highest intensity in the aluminium 2p region is observed at 75.0 eV, but a

significant shoulder is evident, centred at 72.9 eV: these are the 2p<sub>3/2</sub> peaks associated with aluminium atoms in the surface region and in the bulk aluminosilicate network respectively; corresponding 2p<sub>1/2</sub> peaks must be present, but these cannot be observed by inspection. The fitting parameters for the aluminium and silicon 2p regions are summarised in Table 1. At 22.5°, the total areas of the peaks due to surface and bulk aluminium atoms are similar. On increasing the tilt angle to 77.5°, the bulk contribution diminishes, and the surface-associated peaks dominate, with the surface-to-bulk area ratio around 4.54.

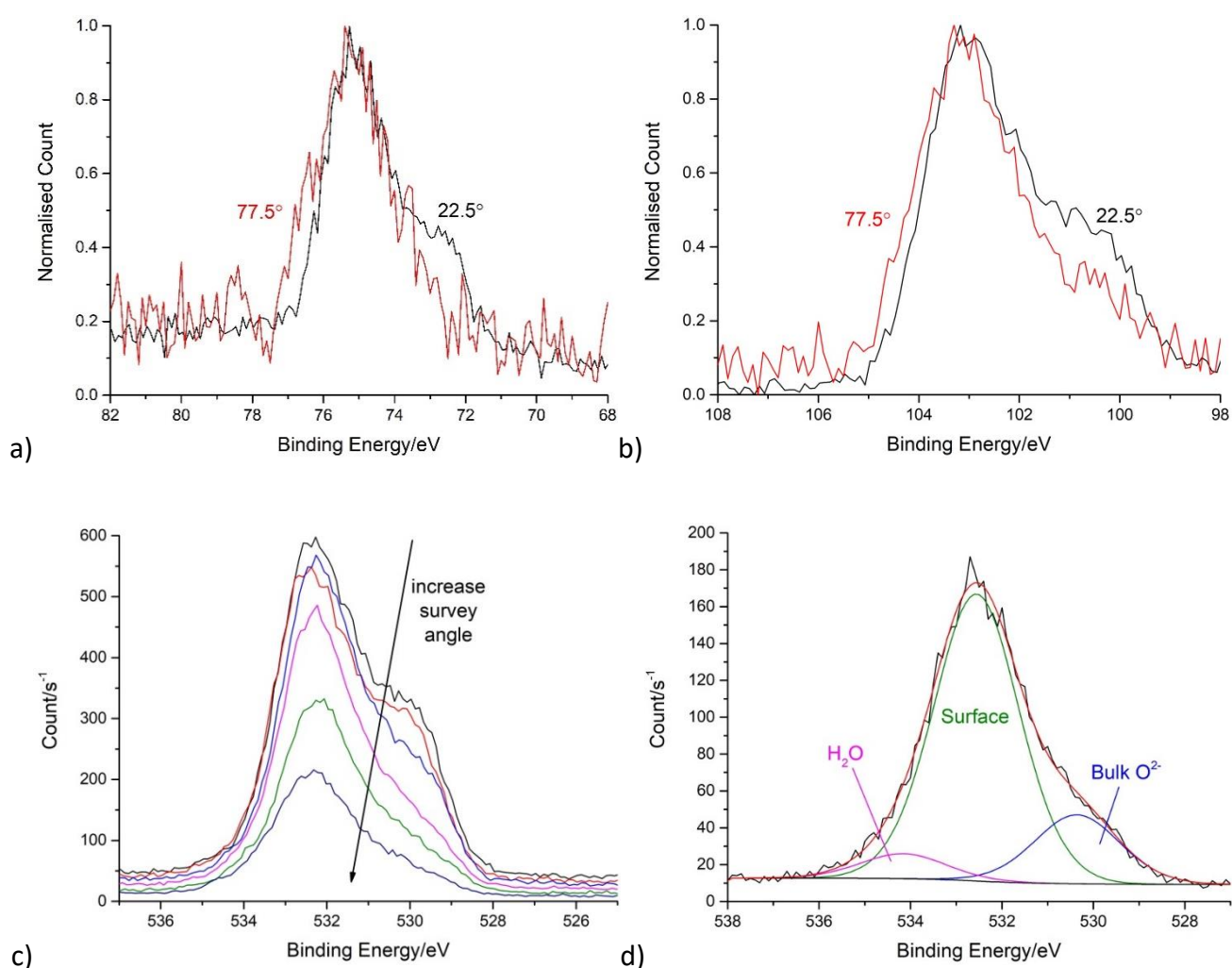


**Figure 2: AR-XP spectra obtained from a polished almandine garnet crystal by varying the tilt angle for a) Al 2p and b) Si 2p regions, at the specified angles, and c) the O 1s region, at 10°**

increments (from 22.5° to 72.5°), and d) fitting of O 1s data, obtained at 77.5° tilt, with the labelled peaks.

The improved surface sensitivity at higher tilt angles is also evident in the silicon 2p region: at normal incidence, the peaks associated with silicon in the bulk aluminosilicate framework (100.7 eV for 2p<sub>3/2</sub>) are also of similar total area to the surface-associated peaks (102.9 eV for 2p<sub>3/2</sub>); at 77.5°, the surface-to-bulk area ratio is around 3.0. Note that the significant splitting of the spin-orbit components in the Fe 2p region (shown in Figure S3 in the Supporting Information) makes quantitative analysis of this part of the spectrum less certain.

**Table 1: XPS Peak Fittings for the Al and Si 2p Regions of Polished Almandine Garnet, at 22.5° and 77.5° Tilts**

Al 2p		Bulk aluminosilicate		Surface region	
		2p <sub>3/2</sub>	2p <sub>1/2</sub>	2p <sub>3/2</sub>	2p <sub>1/2</sub>
Position / eV		72.86	73.66	74.96	75.76
Full Width Half Maximum / eV	22.5°	2.36	2.36	1.47	1.47
	77.5°	1.92	1.92	2.07	2.07
% Area	22.5°	21.0	20.7	29.4	28.9
	77.5°	9.1	9.0	41.3	40.6
Si 2p		Bulk aluminosilicate		Surface region	
		2p <sub>3/2</sub>	2p <sub>1/2</sub>	2p <sub>3/2</sub>	2p <sub>1/2</sub>
Position / eV		100.72	101.35	102.89	103.52
Full Width Half Maximum / eV	22.5°	2.23	2.23	1.67	1.67
	77.5°	2.16	2.16	1.79	1.79
% Area	22.5°	19.2	18.8	31.4	30.7
	77.5°	12.7	12.4	37.8	37.1

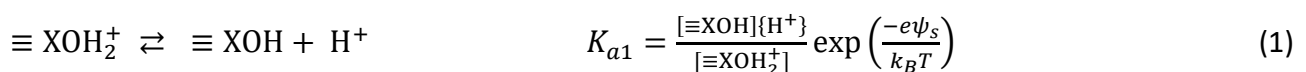
With increasing surveying angle, the main peak in the oxygen 1s region (Figure 2c)) shifts towards higher binding energies, in line with literature observations that surface oxygen species have higher

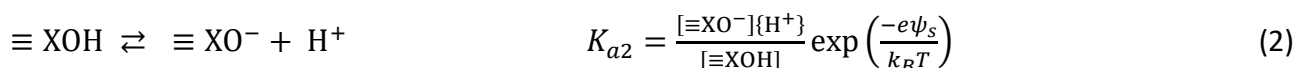
binding energies than those in the bulk.<sup>16,17</sup> The spectrum taken at 77.5° tilt again provides the most prominent surface contribution; fitting of this spectrum is shown in Figure 2 d), and the fitting parameters and peak areas are given in Table 2. The most predominant peak (at 532.6 eV), which increases in intensity at higher tilt angles, is associated with surface oxygen species, whilst the low-binding-energy shoulder (at 530.4 eV) is associated with oxygen in the bulk of the sample. The surface-to-bulk area ratio is 4.2, in general agreement with the corresponding ratios for silicon and aluminium. A third peak (at 534.2 eV) is also identified, corresponding to water adsorbed on the surface; the position of this peak is consistent with literature observations for a hydrated surface.<sup>16</sup>

**Table 2: XPS Peak Fittings for the O 1s Region of Polished Almandine Garnet, at 77.5° Tilt**

Peak	Position / eV	Full Width Half Maximum / eV	Percentage Area / %
Bulk Oxide	530.4	2.20	18.1
Surface Species	532.6	2.20	75.3
Adsorbed Water	534.2	2.20	6.6

To attempt to determine the chemical nature of the surface groups on almandine garnet, we have compiled literature data and looked for any correlation between the binding energies of the oxygen 1s surface XPS peaks of different elemental oxides and the acid dissociation constants ( $pK_a$  values) of the hydroxyl groups that form on these surfaces when exposed to water: the possibility of a correlation appears reasonable, because both the binding energy and the  $pK_a$  values would be expected to be strongly dependent on the electron density around the surface oxygen atom. The acid dissociation equilibria and the corresponding equilibrium constants of the surface groups can be defined as:





$[\equiv \dots]$  and  $\{\dots\}$  denote the concentrations of species on the surface and the activities of species in solution (in mol L<sup>-1</sup>) respectively; X represents the substrate atom to which the surface group is bonded; the exponential terms relate to the change of surface charge on deprotonation ( $e$  is the elementary charge,  $\psi_s$  is the surface potential,  $k_B$  is the Boltzmann constant, and  $T$  is the absolute temperature). Oxides of the components of almandine garnet (iron, aluminium, and silicon) were considered, and manganese and titanium oxides were added to further populate the dataset. Due to the range of values obtained for each element, median binding energies and  $\text{p}K_a$  values were used. The collated results (with references) and correlation graph are shown in Table 3 and Figure 3 respectively.

**Table 3: Median Binding Energies of the O 1s Surface Peaks of Sparingly Soluble Elemental Oxides and their Respective Acid Dissociation Constants**

Oxide Element	Median Binding Energy / eV	Median $\text{p}K_{a1}$	Median $\text{p}K_{a2}$
Manganese	$531.4 \pm 0.3^{18-24}$	-	$6.8 \pm 1.6^{25,26}$
Iron	$531.8 \pm 0.3^{27-30}$	$6.7 \pm 1.3$	$10.1 \pm 1.3^{12,31}$
Titanium	$532.4 \pm 0.7^{32-34}$	$4.4 \pm 2.5$	$6.6 \pm 1.3^{35-37}$
Aluminium	$532.8 \pm 0.7^{16,38-40}$	$1.5 \pm 2.1$	$9.4 \pm 0.7^{28,61}$
Silicon	$533.4 \pm 0.8^{16,43-45}$	$-0.2 \pm 0.1$	$5.8 \pm 2.0^{46-48}$

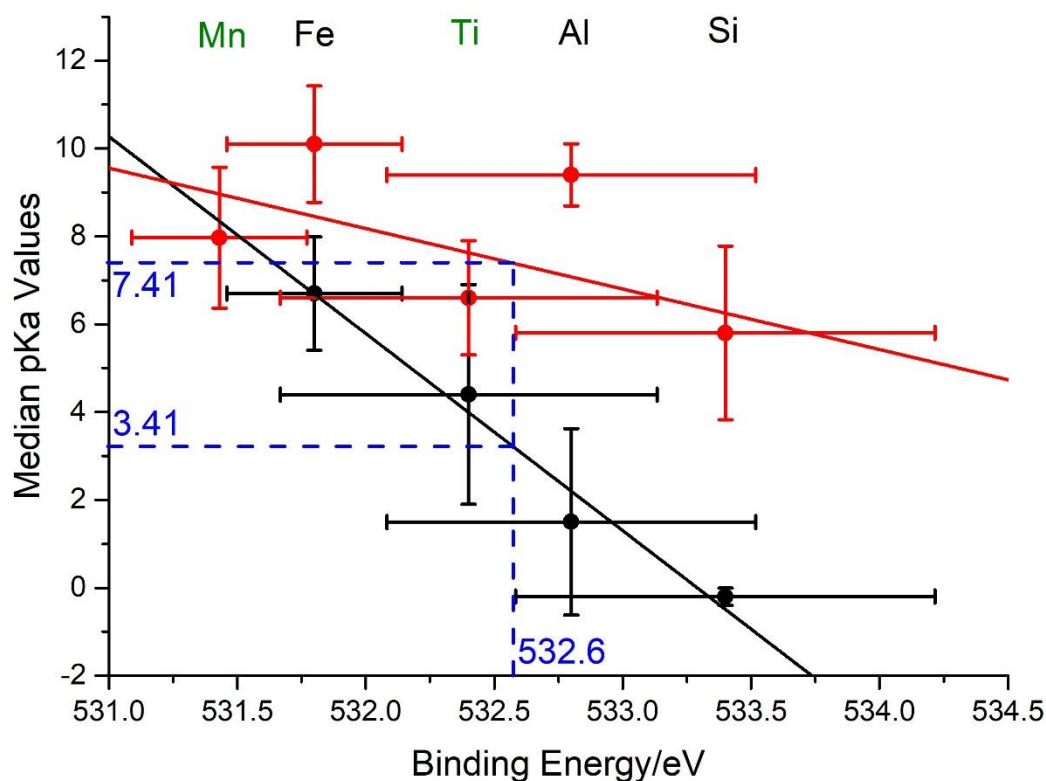


**Figure 3: A plot indicating the relationship between the binding energies of the O 1s XPS surface peaks of different elemental oxides and the  $pK_a$  values of the hydroxyl groups that form on these surfaces (black:  $pK_{a1}$ , red:  $pK_{a2}$ ). The blue dashed line represents interpolation based on the experimentally observed almandine garnet surface peak (at  $77.5^\circ$  tilt). Elements in green are not present in almandine garnet. Error bars indicate the spread of reference data.**

Interestingly, Figure 3 does show a significant correlation ( $R^2 = 0.961$ ) between the median oxide binding energies and the first acid dissociation constant,  $pK_{a1}$ . For the second dissociation constant,  $pK_{a2}$ , the correlation is less strong ( $R^2 = 0.224$ ). Using Figure 3 and the binding energy of the surface oxygen peak observed in ARXPS from almandine garnet (at  $77.5^\circ$  surveying angle), 532.6 eV, the  $pK_a$  values of the surface hydroxyl groups that form on almandine garnet are predicted to be  $3.41 (\pm 0.62)$  and  $7.41 (\pm 0.96)$ . These values will subsequently be compared to  $pK_a$  values obtained from acid-base titration results.

The position of the surface peak in the oxygen 1s region of the almandine garnet XP spectrum differs from the median peaks observed from iron, aluminium or silicon oxide surfaces. This is to be expected: simple bond-counting arguments suggest that fracture of the mineral would be expected to reveal under-coordinated atoms of at least two of the cations (and oxygen) in the surface region, and the XPS data in Figure 2 indicate that surface aluminium, silicon, and oxygen species are all present. In the bulk mineral, each oxygen atom can be considered as bonding to two iron atoms, one aluminium atom, and one silicon atom; fracture could therefore lead to under-coordinated oxygen atoms with up to three of these bonds broken. However, the single surface-related peak in the oxygen 1s region of the XP spectrum suggests that the under-coordinated oxygen atoms in the surface region experience similar chemical environments. It is perhaps most likely that there are oxygen atoms in a range of chemical environments at the surface, but the resolution and surface sensitivity of XPS are inadequate to differentiate these.

It is possible to estimate the thickness of the surface layer based on the relative contributions of surface and bulk XPS peaks. Considering a simple two-layer system, then the ratio of areas of the surface and bulk XPS peaks can be estimated using:

$$\frac{I_{surf}}{I_{bulk}} = \frac{D_{surf}}{D_{bulk}} \left( e^{(t/\lambda \cos \theta)} - 1 \right) \quad (3)$$

where  $D_{surf}$  and  $D_{bulk}$  are the densities of the atom (per unit volume) in the surface layer and the bulk respectively,  $t$  is the thickness of the surface layer,  $\lambda$  is the inelastic mean free path (IMFP) of electrons in the solid (assumed to take the same value in the surface layer and the bulk), and  $\theta$  is the tilt angle between the detector and the surface normal.

If it is assumed that the densities of atoms in the surface layer are approximately unchanged from their bulk values,  $D_{surf} \approx D_{bulk}$ , Equation 3 can be simplified by removing these terms. Taking the

IMFP as 1.1 nm,<sup>17</sup> the surface-to-bulk peak ratios (obtained at known tilt angles) can be used to estimate the surface-layer thickness (the results are shown in Figure S4 in the Supporting Information): averaging these values gives surface-layer thicknesses of 0.63 ( $\pm$  0.17), 0.73 ( $\pm$  0.20), and 0.87 ( $\pm$  0.23) nm for aluminium 2p, silicon 2p, and oxygen 1s respectively. The agreement between these three values suggests that the ratios of the densities of these three atoms in the surface layer to the bulk is similar: this confirms that the surface layer is not depleted of any of these relative to the others, indicating that the cutting, polishing and washing procedure employed did not significantly change the surface composition of the sample.

McCafferty and Wightman have suggested a correction to oxygen 1s XP spectra of native air-formed oxide layers on metal substrates, to remove the contribution of adsorbed oxygen-containing organic species and allow quantitative determination of the concentration of hydroxyl groups in the surface film.<sup>16</sup> Application of the correction in this case would reduce the thickness of the surface layer, calculated using the oxygen 1s region, to 0.34 ( $\pm$  0.11) nm. Analogous corrections are not appropriate for the aluminium and silicon regions, because adsorbed species do not contain these elements. The poorer agreement of the 'corrected' value found using the oxygen region to the surface-layer thicknesses found using the aluminium and silicon regions suggests that the correction factor significantly overestimates the contribution of adsorbed oxygen-containing species in this case. As such, the best estimate of the surface-layer thickness, obtained from the aluminium and silicon photopeaks, is 0.68 ( $\pm$  0.19) nm.

Koretsky and co-workers have described a number of ways in which the densities of surface sites (per unit area) on mineral surfaces can be estimated based on the bulk crystal structure.<sup>49</sup> As garnet does not have a preferred cleavage plane, one would expect to see a number of crystal planes exposed when the mineral fractures. In this case, we use different bulk terminations of {110}

almandine garnet surfaces, and similar methods to Koretsky, to estimate the number of sites present: site densities of the order of  $16 \pm 6$  sites  $\text{nm}^{-2}$  are obtained. The density of oxygen atoms in only the outermost layer of a bulk-terminated almandine garnet {110} surface is  $2.1$  atoms  $\text{nm}^{-2}$ ; one might anticipate that the number of surface sites will be higher than this, with under-coordinated atoms in subsequent layers (but possibly as little as  $0.01$  nm below the outermost layer) expected to be involved in surface reactions when exposed to aqueous solution.

It should also be highlighted that weathering of natural almandine garnet leads to goethite ( $\text{FeO}(\text{OH})$ ) and gibbsite ( $\text{Al}(\text{OH})_3$ ) surfaces.<sup>50</sup> However, in the case of the mined almandine garnet powder used for abrasive blasting, when the selective dissolution and reprecipitation of surface groups has not been possible, the surface chemistry might be expected to more closely resemble that of bulk-terminated garnet, initially formed when the mineral fractures, or the cut-and-polished garnet surface studied here using XPS.

### **Garnet Dissolution Studies**

The dissolution response of acid-washed garnet at strongly acidic pH was first explored to determine the nature of the substrate for subsequent acid-base titrations and variable-pH adsorption experiments. Figure 4 shows the masses of almandine garnet and calcium carbonate dissolved (inferred from ICP-OES data of the dissolved aluminium and calcium ions respectively) with increasing equilibrium time at pH  $1.98 (\pm 0.09)$ . It is evident that almandine garnet initially dissolves quickly (approximately  $0.13$  g out of  $2.0$  g of almandine garnet has dissolved after 36 minutes), but only a small increase is seen in the mass dissolved at timescales of the order of several days. Therefore, for experiments that involve garnet in very acidic environments, the role of dissolved ions from the mineral must be considered in the equilibrium system.

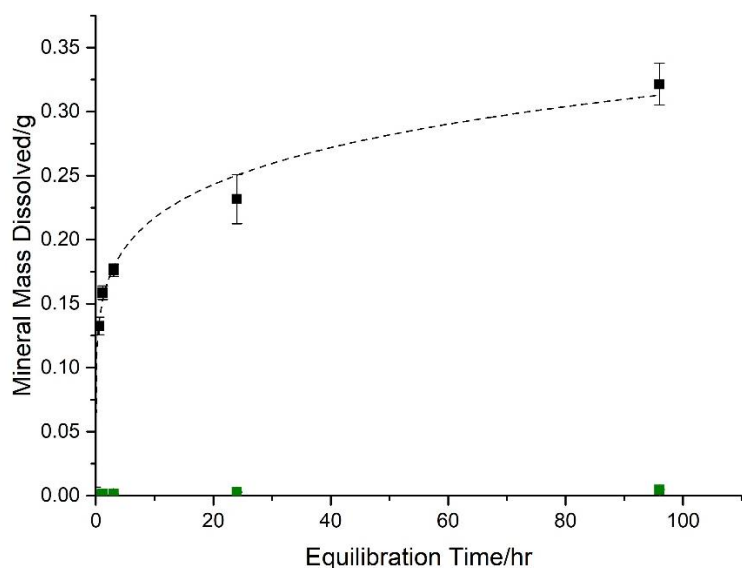


**Figure 4: The masses of almandine garnet (black) and CaCO<sub>3</sub> (green) dissolved from 2.0 g acid-washed almandine garnet powder with increasing time at pH 2, in 100 mM NaNO<sub>3</sub> solution. Error bars represent experimental and dilution errors of each sample.**

As was reported previously,<sup>5</sup> analysis of the washings obtained during the acid-washing procedure indicated that significant levels of dissolved aluminium and calcium ions are present in the initial (10 %/wt nitric acid) washings, but the levels decrease on subsequent washes with ultrapure water, such that on the fourth, fifth, and sixth washes, no dissolved ions from the mineral can be detected. However, dissolution of almandine garnet has recently been noted over a wide pH range, including in ultrapure water.<sup>13</sup> Therefore, to further assess the extent to which dissolution of garnet could occur under our experimental conditions, we have obtained ICP-OES data quantifying the levels of dissolved iron, aluminium, and silicon present in the supernatant after 4 g acid-washed garnet powder was tumbled in 20 ml ultrapure water, 0.1 M hydrochloric acid, or 0.1 M sodium hydroxide for one week; these data are shown in Table S2 in the Supporting Information.

Although dissolved iron, aluminium, and silicon were present in all samples, the concentrations measured were relatively low, even in strong acid and strong base (final pH of 2.0 ( $\pm$  0.5) and 12.0

( $\pm 0.5$ ) respectively): the highest observed concentration was for silicon after the garnet had been tumbled in 0.1 M sodium hydroxide, and this was equivalent to an estimated 1.5 % of the silicon initially present having dissolved; in ultrapure water (final pH of 5.1 ( $\pm 0.2$ )), which is closer to the pH range relevant to most of our subsequent experiments, the value is just 0.05 %. PXRD data from the solids obtained from these samples, described previously, indicate that dissolution of the garnet powder, followed by precipitation of other phases, for example metal hydroxides, does not occur to measurable levels. Although the sensitivity of PXRD to changes in the surface composition is low, more conclusive evidence comes from the acid-base titration data, which will be described subsequently. One would expect to see additional inflection points in the data, characteristic of dissolution and precipitation of phases (especially as the increments of base addition were small, 10  $\mu\text{L}$ ); no such features are observed. We can therefore be confident both that dissolution of the garnet powder does not significantly alter its specific surface area and that the low levels of dissolved ions from the mineral will not affect our aqueous solution equilibria experiments.

Given the different solubilities of the metal ions, it is difficult to assess whether there is preferential dissolution of one or more of the elements, which could alter the nature of the surface groups present over the pH range of interest. Comparing the number of dissolved silicon atoms per unit surface area at high pH (9.7  $\text{nm}^{-2}$ ), to the previous estimate of the number of surface sites (16  $\pm 6$   $\text{nm}^{-2}$ ), it is clear that this extent of dissolution could change the distribution of different surface groups present, if there is preferential dissolution. However, it should again be emphasized that the vast majority of our aqueous solution equilibria experiments are over significantly shorter times and at more moderate pH: previous data have shown that the dissolution rate (under flow conditions) drops by over an order of magnitude between pH 12 and the minimum around pH 5.<sup>13</sup> Although we cannot conclusively rule out the possibility that the numbers of different surface sites present changes over the range of interest, we do not have any evidence that directly suggests this,

and the absence of additional features in the acid-base titration data suggests that any dissolution of surface groups and reprecipitation of other phases is minimal. We therefore proceed by attempting to utilise the simplest models possible to rationalise the behaviour observed, with fixed numbers of surface sites.

Figure 4 also shows that very little calcium dissolves into the acidic solution, even after several days. We conclude therefore that the initial acid washing procedure was sufficient to remove any calcium carbonate impurities and that leaching of calcium from the garnet itself is unlikely to be significant. At higher pH, the lower solubility of calcium ions will further reduce the likelihood. Therefore, for numerical modelling of our experimental data on the behaviour of calcium ions in neutral and mildly basic solutions, the dissolution of calcium carbonate can be considered to be negligible.

### **Salt-Solution Titrations**

When 5 g acid-washed almandine garnet powder is added to 50 ml ultrapure water, the measured pH is 4.93 ( $\pm 0.08$ ). The solid blue, black, and green lines in Figure 5 show the subsequent change in the measured pH as 100 mM sodium, magnesium, or calcium nitrate respectively is added in 0.001 or 0.002 mL aliquots. It is evident that in all three cases, the pH of the garnet suspension decreases on the addition of the salt solution; no systematic change in pH is observed when the salt solution is added to a blank solution, without acid-washed garnet powder.

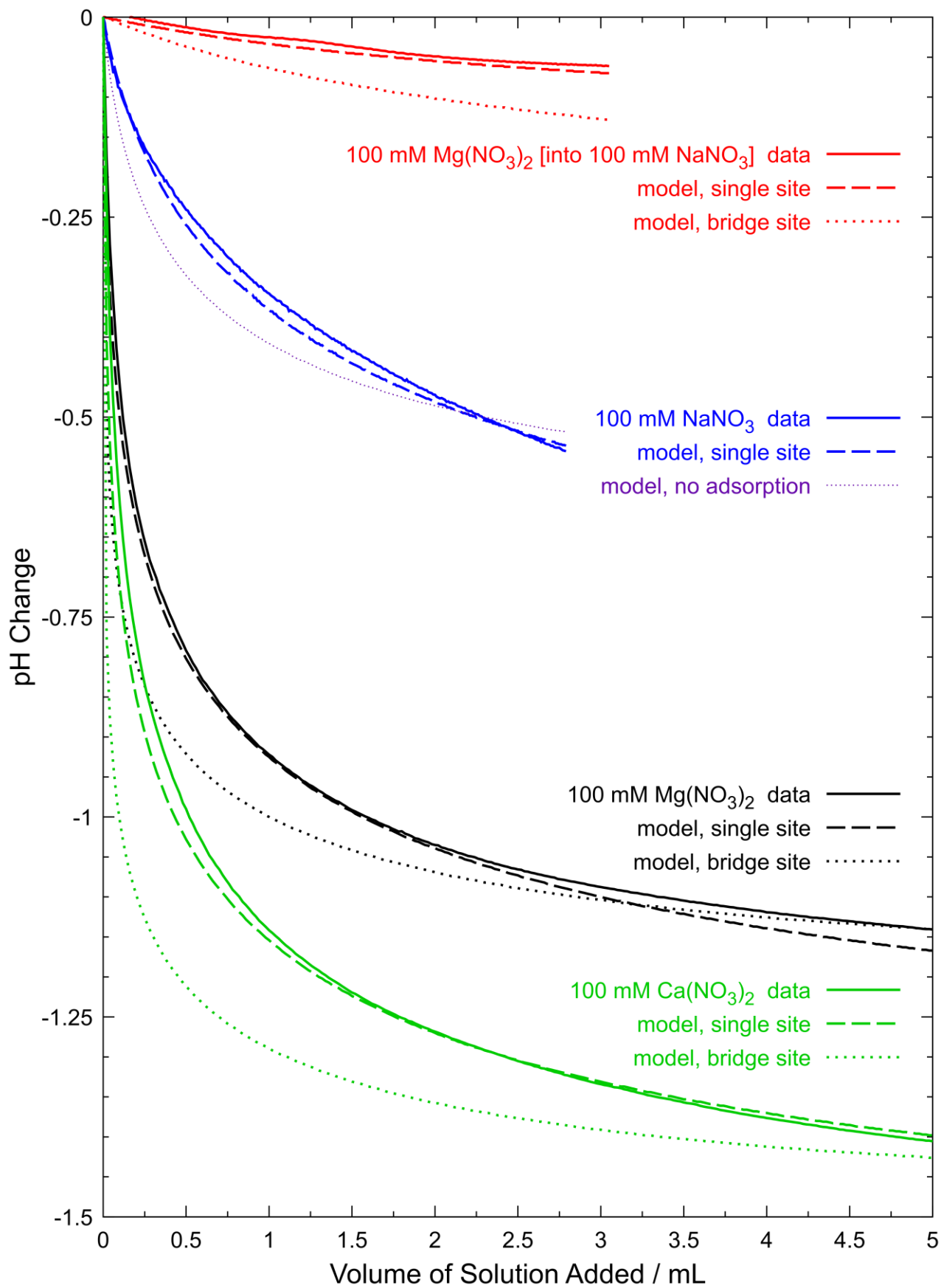
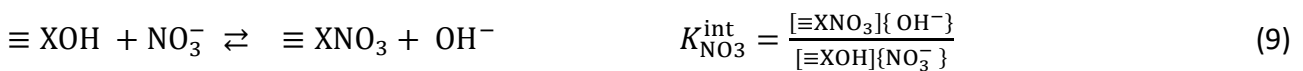
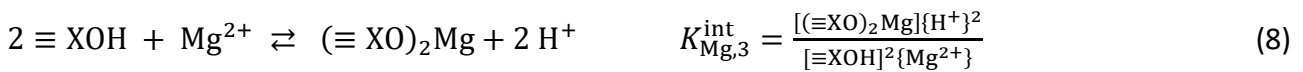
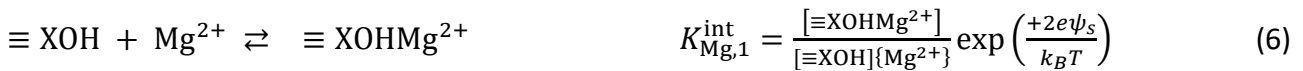
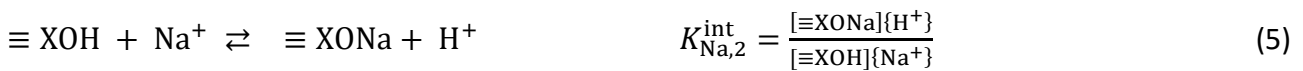


Figure 5: The pH change when 100 mM NaNO<sub>3</sub> (blue), Mg(NO<sub>3</sub>)<sub>2</sub> (black) or Ca(NO<sub>3</sub>)<sub>2</sub> (green) is added in 0.001 or 0.002 mL aliquots to 5 g acid-washed garnet powder in 50 mL ultrapure water, and when 100 mM Mg(NO<sub>3</sub>)<sub>2</sub> is added to acid-washed garnet powder in 50 ml 100 mM NaNO<sub>3</sub> (red). Solid lines indicate experimental data; dashed and dotted lines indicate predictions from numerical modelling, using equilibria of the form of Equations 4 (or 2 for sodium) and 5 respectively, with the exception of the purple line, which indicates the prediction when specific adsorption of Na is not considered.

When the mineral is added to ultrapure water, the predominant surface species are likely to be neutral hydroxyl groups ( $\equiv \text{XOH}$ , where X now represents the substrate atom(s), Fe, Al, and/or Si, to which the group is bonded). When salt solutions are then added, various equilibria involving the surface groups are conceivable that could lead to the direct adsorption of ions (into the Stern layer). For example, for the monovalent sodium cation, the divalent magnesium (or calcium) cation, and the monovalent nitrate anion, the simplest equilibria (and corresponding equilibrium constants,  $K^{\text{int}}$ ) are:



The terms involved were defined for Equations 1 and 2. The equilibria listed indicate modes of adsorption in which ions bind directly to individual surface sites, except for Equation 8, where the cation bridges between two surface sites; other (more complex) adsorption equilibria are also possible.

The decreases in pH observed when the salt solutions are added to the garnet suspension are consistent with the cations adsorbing to the surface and displacing protons into solution (for example, according to Equations 5, 7, and 8); this appears to dwarf any adsorption of the nitrate anion (Equation 9), which would displace hydroxide ions into solution and result in an increase in pH. However, the decrease in pH as the salt solution is added will depend on the mode of adsorption, in addition to the number of surface sites present and the strength of binding. We have therefore employed numerical modelling to predict the pH change for different adsorption equilibria, site densities, and equilibrium constants, to compare to experimental data and try to determine the dominant mechanism, the number of sites and the strength of binding at the garnet surface.

The dashed lines in Figure 5 indicate the predicted pH changes from numerical modelling of cation adsorption to the garnet surface, using equilibria of the form of Equation 5 for sodium (blue), and of the form of Equation 7 for magnesium (black) and calcium (green). The dotted black and green lines indicate the predicted pH change if the divalent cations were to bind to the surface according to Equation 8 (or the equivalent form for calcium), effectively in a bridging mode between two surface sites. The dashed lines show very good agreement with the experimental data (root-mean-square error (RMSE) values of 0.02 for both magnesium and calcium), but the dotted black and green lines clearly fit less well (RMSE values of 0.06 for calcium and 0.11 for magnesium), indicating

that modes of adsorption in which each cation binds to a single surface site, displacing one proton, appear to be preferred.

Although the specific surface area for acid-washed garnet powder has been found (from BET isotherm) to be  $5.54 (\pm 0.03) \text{ m}^2 \text{ g}^{-1}$ , we do not have direct experimental evidence for the number of cation binding sites on the surface. As such, a range of site densities ( $n_s$ ) were tested using numerical modelling, with the strength of binding ( $K^{\text{int}}$ ) adjusted in each case in order to optimise the fit to the experimental data. Interestingly, it is observed that effectively identical fits (those indicated by the dashed lines in Figure 5) can be obtained for any choice of site density above 1 site  $\text{nm}^{-2}$  for calcium, 0.3 sites  $\text{nm}^{-2}$  for magnesium, and 0.1 sites  $\text{nm}^{-2}$  for sodium. Below these values, there are insufficient surface sites to which cations can bind in order to release the protons required for the experimentally observed pH change; therefore, these values can be considered as a lower-bound for the number of cation binding sites on the garnet surface.

Figure S5 of the Supporting Information indicates the different numbers of surface binding sites  $\text{nm}^{-2}$  ( $n_s$ ) that were tested and could fit the experimental data, and the values of the equilibrium constant ( $K^{\text{int}}$ ) required to give the optimal fits in each case. From this graph, it is observed that the value of  $K^{\text{int}}$  needed to give the best fit is related to  $n_s$  (above the previously mentioned lower bounds) according to:

$$K^{\text{int}} = (10^x n_s)^{-1} \quad x = 4.80 \text{ (Na)}, 3.09 \text{ (Mg)}, 2.41 \text{ (Ca)} \quad (10)$$

Although the fundamental origin of this empirically-derived relationship is unclear, the increasing value of  $x$  on going from sodium, to magnesium, to calcium is indicative of an increase in the strength of binding, if the number of sites is identical for the different cations.

The observed weak binding of sodium to the garnet surface is unsurprising; in fact, sodium is considered to be effectively inert to direct reaction with many surfaces.<sup>51</sup> We therefore consider an alternative possibility, that the deprotonation of surface groups observed (via the drop in pH) when sodium nitrate is added to garnet powder is not due to sodium binding to surface sites directly, but instead results from the increasing ionic strength of the solution (which makes the formation of a highly charge surface more favourable) facilitating the deprotonation to give negatively charged surface groups, according to Equation 2.

Although it is not straightforward to separate the two factors (ions added to the solution increase the ionic strength and may also bind specifically to the surface), numerical modelling has been used to compare the cases where direct binding of sodium to the surface is considered (the dashed blue line in Figure 5, discussed previously) and where no specific binding of sodium occurs, but only deprotonation of the surface groups according to Equation 2 (the dotted purple line in Figure 5). The deprotonation-only model predicts a steeper decrease in pH than that predicted when specific adsorption is considered, fitting the data somewhat less well (the RMSE value is 0.05, compared to 0.014 when specific adsorption is considered); however, both fits appear reasonable, and so we cannot conclude definitely on this evidence alone that sodium binds specifically to the garnet surface.

To attempt to assess whether the different cations bind specifically to the same surface sites, the pH change was monitored as 100 mM magnesium nitrate was added in 0.002 mL aliquots to acid-washed garnet powder in 100 mM sodium nitrate; this is shown by the solid red line in Figure 5. It is evident that the change in pH in this case is significantly smaller than when the magnesium nitrate is added to acid-washed garnet powder in ultrapure water, supporting the hypothesis that the magnesium and sodium ions bind to the same surface sites: the small change in pH is consistent

with the more strongly binding divalent cation displacing protons from additional sites, whilst also displacing some of the previously bound sodium ions.

The dashed and dotted red lines in Figure 5 indicate the predicted pH change from numerical modelling, with both cations binding to the same surface sites (sodium binding according to Equation 5 and magnesium according to Equation 7 (dashed line) or Equation 8 (dotted line), and with the equilibrium constants obtained from the individual salt-solution titrations, as described above). Although these data appear to slightly favour a bridging mode of adsorption for magnesium (the RMSE value is 0.007, compared to 0.05 when magnesium binds to single sites), the agreement between both predictions and the experimental data is reasonable, further supporting the hypothesis that the different cations bind to the same surface sites.

One final aspect that should be considered when interpreting the salt-solution titration data is that, for the divalent cations, the pH decrease could be a consequence of both adsorption (e.g. Equation 7) and deprotonation of additional surface groups (Equation 2), which would reduce the extent to which the surface charge increases. This scenario is distinct from bridging adsorption (Equation 8), because there would not need to be a particular stoichiometric ratio between the number of cations adsorbed and the number of protons released (although a 1:1 ratio of the processes indicated in Equations 7 and 2 would ensure that the surface remains neutral overall, which would be expected to be particularly favourable at low ionic strength). However, numerical modelling does not support this hypothesis: the predicted decrease in pH when both equilibria are included is again steeper than that observed experimentally.

### **Adsorption Isotherms**

Although measuring the decrease in the solution concentration of an ion provides an alternative method of monitoring its adsorption onto a surface, it is important to remember that in addition to

specific adsorption to surface sites, accumulation of ions in the diffuse layer is possible, balancing the charge at the surface (including the Stern layer).<sup>52</sup> As such, adsorption isotherms are often recorded in relatively high concentrations of an effectively inert electrolyte: if the ionic strength is high and effectively unchanging, then the length of the diffuse layer is constant and small. In the case of acid-washed almandine garnet powder, salt-solution titrations indicated that sodium binds significantly less strongly than magnesium or calcium, whilst there was no indication of nitrate adsorption. Therefore, 100 mM sodium nitrate was used as the electrolyte for magnesium and calcium adsorption isotherms.

Experimental adsorption isotherm data for magnesium (black) and calcium (green) are shown by the points in Figure 6: variable- and constant-pH data are shown in the upper and lower plots respectively. The constant-pH data were obtained at equilibrium pH of 9.35 ( $\pm$  0.05) in order to avoid the possibility of metal hydroxide precipitation at higher pH (especially the sparingly soluble magnesium hydroxide),<sup>53</sup> which would make quantitative measurement of the adsorption through solution-depletion impossible. As expected, the variable-pH data show that the adsorption of the cations becomes significant at high pH,<sup>12,54</sup> and the constant-pH data indicate that the adsorption increases (at a decreasing rate) with the solution concentration of the cation. Consistent with what was observed in salt-solution titrations, it is evident from both the lower pH value at which the adsorption 'step' occurs in the variable-pH data and the steeper rise and higher plateau in the constant-pH data that calcium adsorbs more strongly than magnesium.

The dotted lines in Figure 6 indicate the adsorption of magnesium or calcium to the garnet surface predicted by numerical modelling, given the experimental concentrations and using the equilibria and equilibrium constants (for sodium, magnesium, and calcium adsorption) that provided the best fits for the salt-solution titration results, as discussed previously, with 1 surface adsorption site nm<sup>-2</sup>

<sup>2</sup>; this site density was used because it was the lower-bound for the number of sites that could fit the pH changes observed in the salt-solution titration experiments. However, it is evident that in this case the predictions fit the experimental data very poorly, significantly underestimating the adsorption of magnesium or calcium.

In fact, the best fits that can be obtained to the adsorption data (whilst still obeying Equation 10, and therefore fitting the salt-solution titration data) occur with 40 surface sites nm<sup>-2</sup>: the solid lines in Figure 6 indicate the predicted adsorption with this site density (and with the corresponding equilibrium constants, 10<sup>-6.4</sup>, 10<sup>-4.7</sup>, and 10<sup>-4.0</sup> for sodium, magnesium, and calcium respectively). It is evident that, especially in the case of magnesium, the predictions still do not reproduce the experimental data well: the RMSE values for the variable-pH isotherm are 24 and 5 % for magnesium and calcium respectively (compared to 38 and 39 % with 1 site nm<sup>-2</sup>); for the constant-pH isotherm, the values are 0.22 and 0.19 μmol m<sup>-2</sup> for magnesium and calcium respectively (compared to 0.9 and 1.5 μmol m<sup>-2</sup> with 1 site nm<sup>-2</sup>).

In addition, the required surface site density of 40 nm<sup>-2</sup> seems implausibly high, when compared to the surface site densities estimated previously: 16 ± 6 nm<sup>-2</sup> (from different terminations of {110} almandine garnet surfaces) and 2.1 nm<sup>-2</sup> (the density of oxygen atoms in only the outermost layer of a bulk-terminated almandine garnet {110} surface). The poor fit of the predictions from the numerical model to the adsorption data indicates that it is not possible to fully describe the behaviour of a surface as complex as that of almandine garnet using such a simple two-layer model, with just one type of surface site. The greater complexity of the adsorption reactions occurring and the presence of multiple types of adsorption site are also suggested by additional data, which we will now consider.

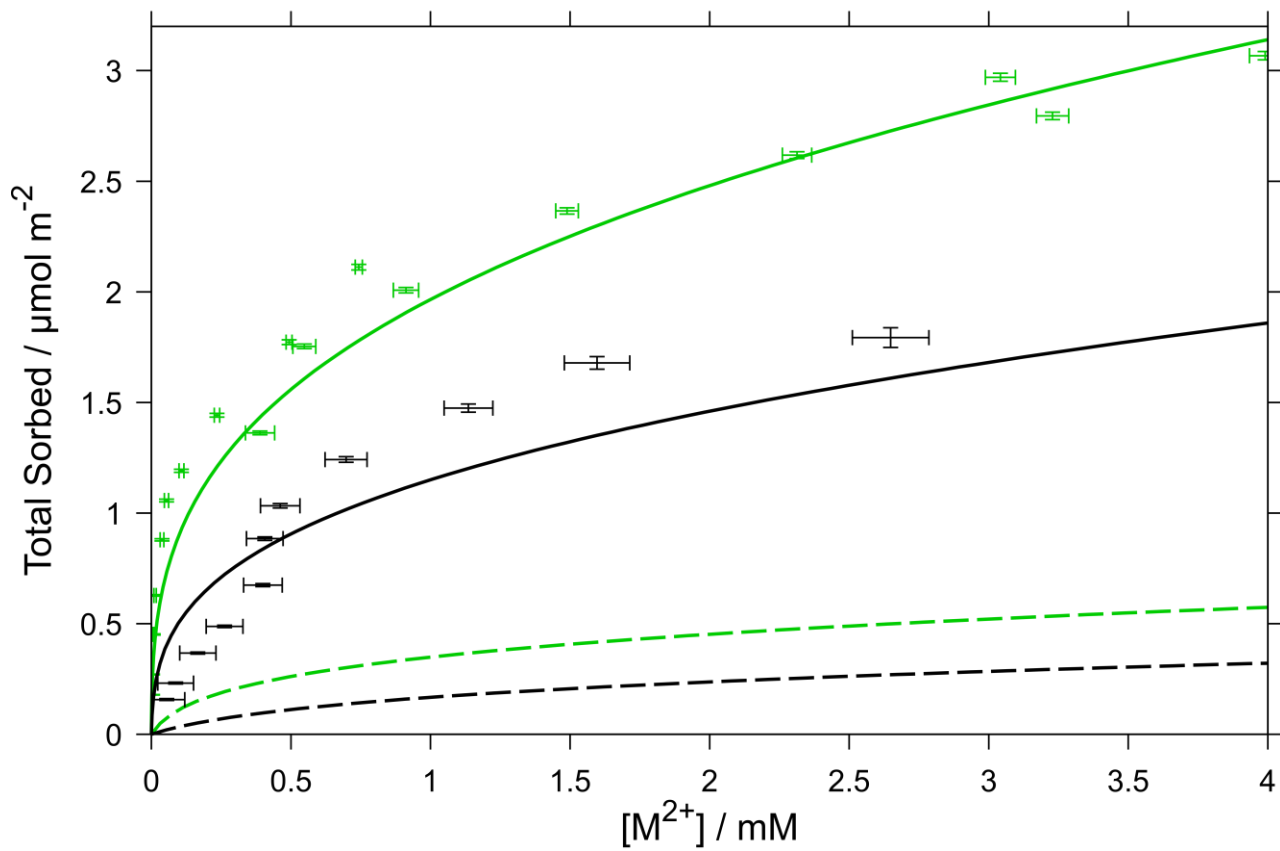
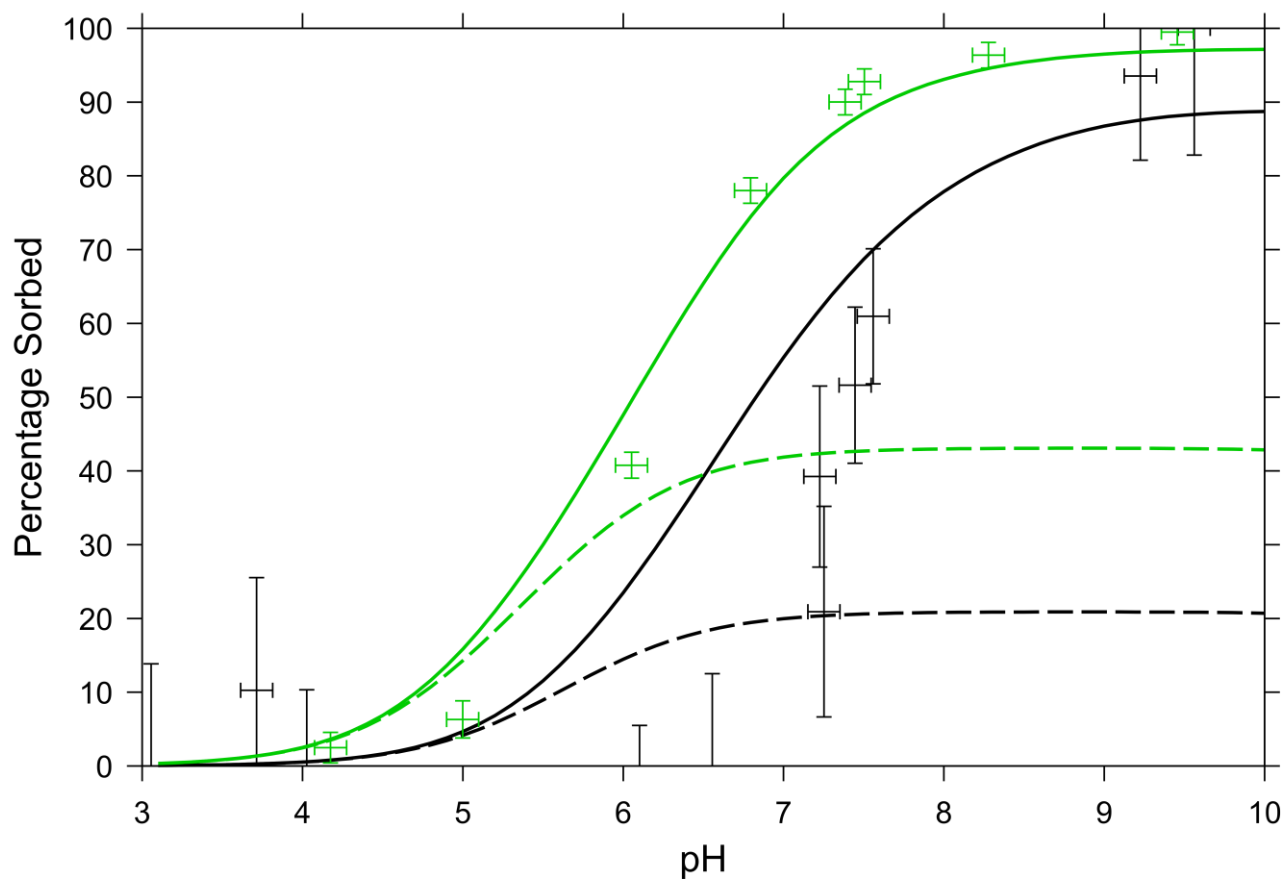


**Figure 6: Solution-depletion adsorption isotherms of Mg (black) and Ca (green) onto 200 g L<sup>-1</sup> acid-washed garnet powder in 100 mM NaNO<sub>3</sub>. Top: variable-pH isotherm, obtained with 0.5 mM Mg(NO<sub>3</sub>)<sub>2</sub> or Ca(NO<sub>3</sub>)<sub>2</sub>; bottom: constant-pH isotherm, obtained at pH 9.35 (± 0.05). In both cases, the pH was adjusted by adding 100 mM NaOH or HNO<sub>3</sub> in 100 mM NaNO<sub>3</sub>. Points indicate experimental data; lines are predictions from numerical modelling, using binding constants determined from salt-solution titrations with 1 (dashed lines) or 40 (solid lines) sites nm<sup>-2</sup>. Note that 1 μmol m<sup>-2</sup> = 0.60 nm<sup>-2</sup>. Error bars represent experimental and dilution errors of each sample.**

Plots of the number of moles of base added to maintain the pH in the constant-pH isotherms (at 9.35 (± 0.05)) against the number of moles of magnesium or calcium adsorbed are shown in Figure 7. The plots are linear, suggesting that in both cases the cation-adsorption mechanism does not change significantly over the range studied: if the cations were to adsorb to bridging or individual sites dependent on coverage, one might expect to see a change in the gradient; similarly, the linearity appears to rule out the possibility that the surface is significantly negatively charged at pH 9.35 in 100 mM sodium nitrate, which would allow added divalent ions to adsorb without displacing protons. However, the gradients of the best-fit lines differ: 1.58 (± 0.08) protons are displaced for every magnesium ion adsorbed, but for calcium the number is 1.03 (± 0.04), suggesting that different adsorption mechanisms could occur for the two cations.

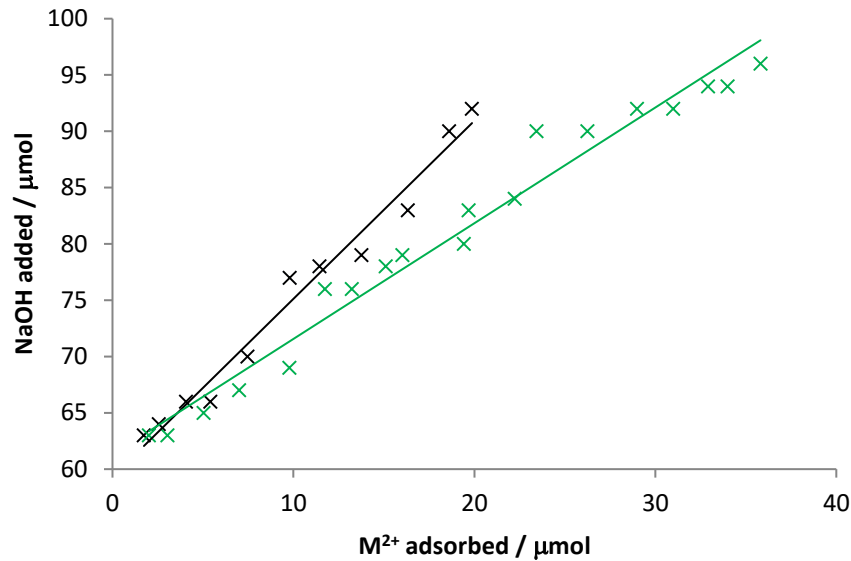


**Figure 7: The number of moles of NaOH added to maintain the pH at  $9.35 (\pm 0.05)$  against the number of moles of Mg (black) or Ca (green) adsorbed in the constant-pH isotherm experiments.**

Numerical modelling using equilibrium constants from the salt-solution titrations predicts gradients around 0.12 in both cases. The small predicted gradient is a consequence of the fact that, in 100 mM sodium nitrate, over 90 % of surface sites would be expected to have sodium adsorbed, and so when the more strongly binding magnesium or calcium adsorbs, it is mainly sodium that is displaced. Clearly, the higher observed number of protons displaced suggests that the role of adsorbed sodium is much less significant. But removing the competition for adsorption sites between sodium and the divalent cations from the numerical model prevents the variable- and constant-pH isotherm data from being fitted satisfactorily using self-consistent binding-site densities and equilibrium constants.

Previous work studying hydrous ferric oxide predicted that between 1.7 and 2.0 protons would be displaced from the surface for each zinc ion adsorbing, dependent on pH and solution ionic strength.<sup>12</sup> The value for the adsorption of magnesium on garnet,  $1.58 (\pm 0.08)$ , is in general agreement with this, further suggesting that sodium nitrate is effectively an inert electrolyte (or, at

least, that protons, not sodium, are the main ions displaced when magnesium adsorbs). However, the significantly lower value observed for calcium,  $1.03 (\pm 0.04)$ , is somewhat surprising and could indicate that different adsorption mechanisms occur for the two divalent cations, with a more significant change in the surface charge on adsorption of calcium than magnesium.

Further indication that the adsorption mechanism for calcium could differ from that for magnesium comes from the shape of the two constant-pH isotherms. Langmuir-type adsorption, which assumes a fixed number of surface sites and that adsorption at a given site is independent of the occupancy of adjacent sites, can be described using an expression of the form:

$$\frac{\theta}{\theta_{sat}} = \frac{Kc}{1+Kc} \quad (11)$$

where  $\theta$  and  $\theta_{sat}$  are respectively the amount of the species adsorbed and the amount adsorbed at saturation,  $c$  is the concentration of the species in solution at equilibrium, and  $K$  is the Langmuir constant. From Equation 8, it can be seen that if adsorption is Langmuirian, a plot of  $\theta^{-1}$  versus  $c^{-1}$  will be linear, with intercept equal to  $\theta_{sat}^{-1}$  and gradient equal to  $(K\theta_{sat})^{-1}$ . Plots of this form, derived from the constant-pH adsorption data for magnesium (black) and calcium (green) on acid-washed garnet, are shown by the points in Figure 8.

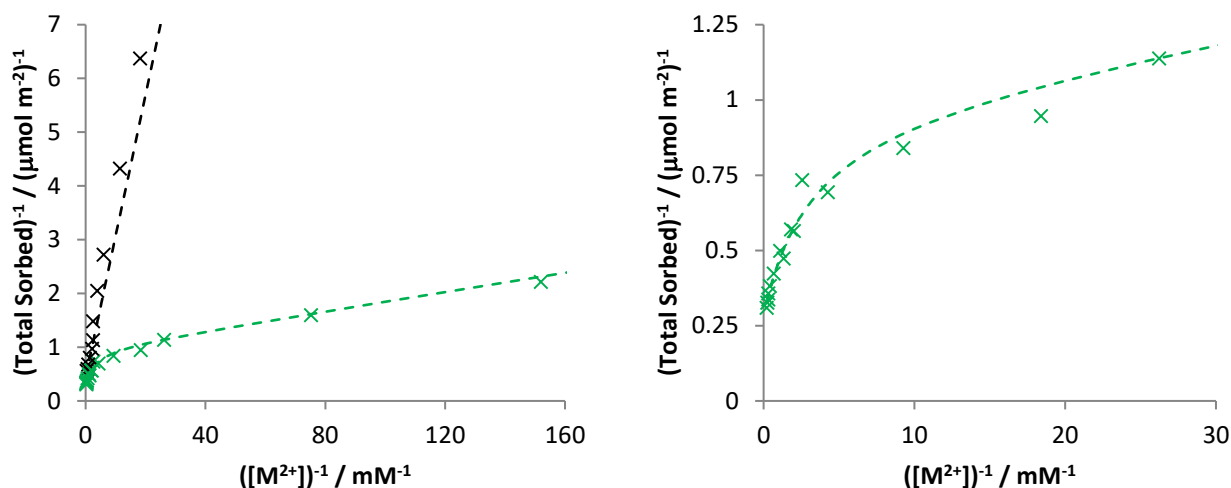


**Figure 8: Plots to determine whether the constant-pH isotherm data for the adsorption of Mg (black) or Ca (green) on acid-washed garnet powder exhibits Langmuir-type behaviour. Points indicate data; dashed lines indicate Langmuir-type fits, using the parameters described in the text (with one type of surface site for Mg adsorption and two independent types of site for Ca). The right-hand plot covers a smaller range, to highlight the non-linearity of the Ca data.**

In the case of magnesium, the data in Figure 8 are close to linear ( $R^2 = 0.991$ ; the minor deviation is most likely due to experimental error), as would be expected for Langmuir-type behaviour. The total magnesium adsorbed at saturation is  $2.3 \mu\text{mol m}^{-2}$  (equivalent to approximately  $1.4 \text{ nm}^{-2}$ ), and the Langmuir constant is  $1.68 \text{ mM}^{-1}$ . By contrast, for calcium the plot is not a straight line: the gradient appears to change dramatically at around  $2.5 \text{ mM}^{-1}$ . The data for calcium can be fitted using a Langmuir model (the dashed green line in Figure 8), if two independent types of surface sites are considered, that adsorb  $1.0$  and  $2.5 \mu\text{mol m}^{-2}$  ( $0.6$  and  $1.5 \text{ nm}^{-2}$ ) calcium ions with Langmuir constants  $113$  and  $0.880 \text{ mM}^{-1}$  respectively; this implies that the minority sites adsorb the calcium ions significantly more strongly than the majority sites, a phenomenon also suggested for calcium adsorption on hydrous ferric oxide.<sup>12</sup>

However, although the best Langmuir-type fit to the constant-pH calcium adsorption data is obtained with two different types of surface sites, the linearity of the sodium-hydroxide-added versus cation-adsorbed plot (Figure 7) indicates that the same number of protons ( $1.03 \pm 0.04$ ) are displaced for all calcium ions adsorbed. It is interesting that if the number of protons displaced per cation adsorbed is multiplied by the total number of cations adsorbed at saturation (according to the Langmuir fits of the data obtained at pH  $9.35 \pm 0.05$ ), the result is  $3.6 \mu\text{mol m}^{-2}$ , or  $2.2 \text{ nm}^{-2}$ , for both magnesium and calcium; this suggests that the number of protons that can be displaced from the surface may determine the number of the different cations that can adsorb at constant pH.

Figure 9 shows the constant-pH isotherm data, with different methods of fitting. It is evident that the Langmuir-type fits (dashed lines) more closely reproduce the experimental data than do the best fits obtained from the numerical modelling: the RMSE values are  $0.11$  and  $0.12 \mu\text{mol m}^{-2}$  for magnesium and calcium respectively (compared to the  $0.22$  and  $0.19 \mu\text{mol m}^{-2}$  from numerical modelling with  $40 \text{ sites nm}^{-2}$ ); this further suggests that the two-layer model does not fully describe the behaviour in this complex system. It is also noteworthy that, as previously discussed, the density of oxygen atoms in only the outermost layer of a bulk-terminated almandine garnet  $\{110\}$  surface is  $2.1 \text{ atoms nm}^{-2}$ , much closer to the number of surface sites predicted by the Langmuir-type fits than the  $40 \text{ sites nm}^{-2}$  from numerical modelling with the two-layer model.

We also note that it is possible to accurately fit the total calcium adsorbed (in  $\mu\text{mol m}^{-2}$ ) with the expression  $2.1c^{0.281}$  (where  $c$  is the equilibrium concentration in mM); this is indicated by the red dotted line in Figure 9 (for which the RMSE value is  $0.11 \mu\text{mol m}^{-2}$ , slightly lower than the  $0.12 \mu\text{mol m}^{-2}$  from the calcium Langmuir-type fit). Although such an empirically determined, Freundlich-type fit seemingly offers little mechanistic information about the adsorption process, the small value of

the power to which  $c$  is raised (0.281) indicates that adsorption of calcium quickly becomes less favourable as the coverage increases. This observation is consistent with the surface becoming increasingly positively charged as calcium ions adsorb, but with only one proton displaced for each ion that binds (as shown by Figure 7).

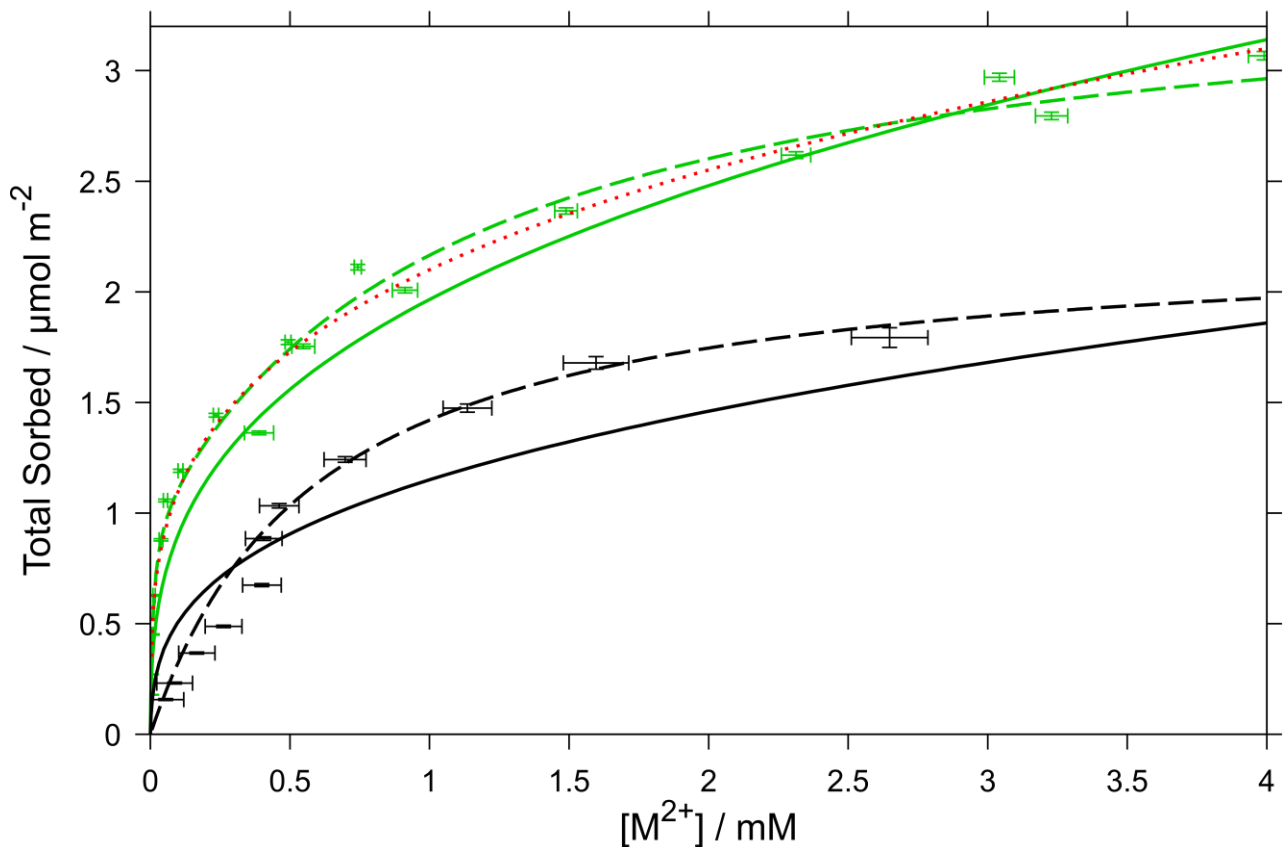
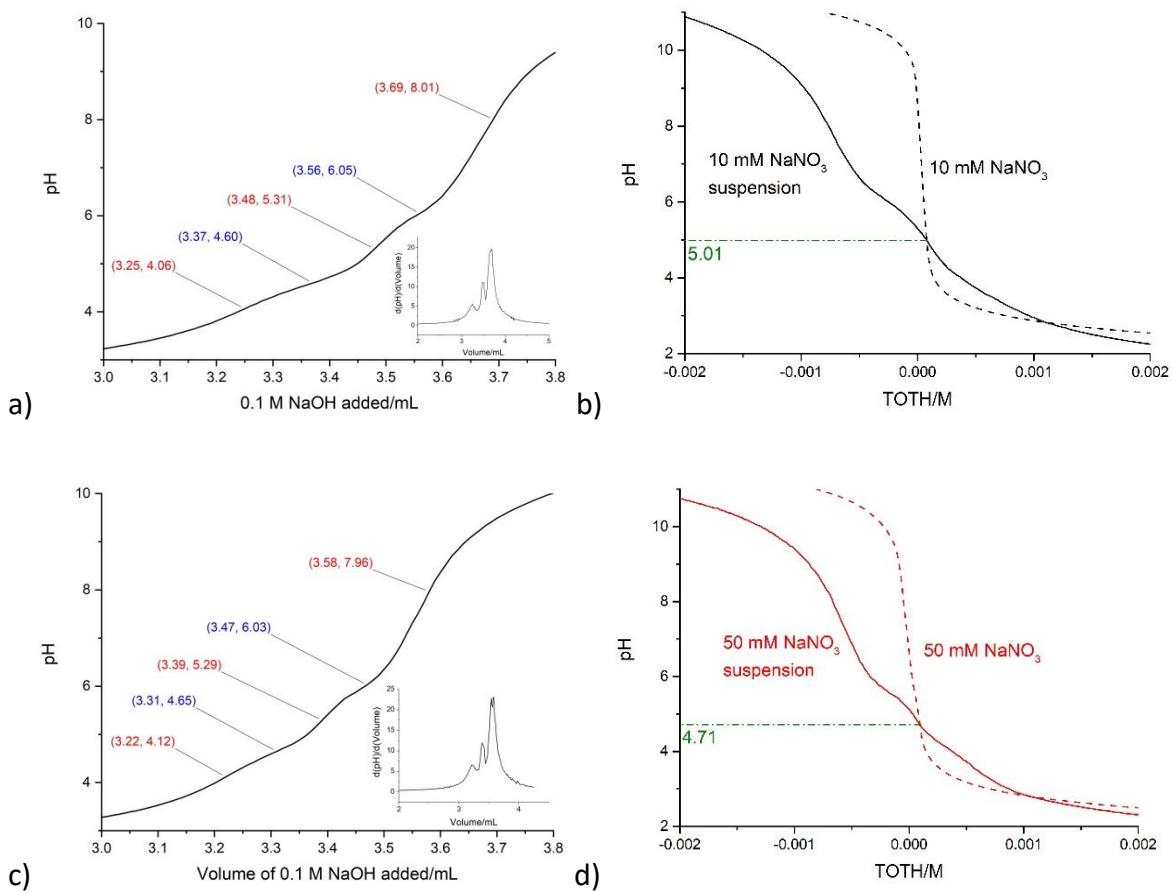
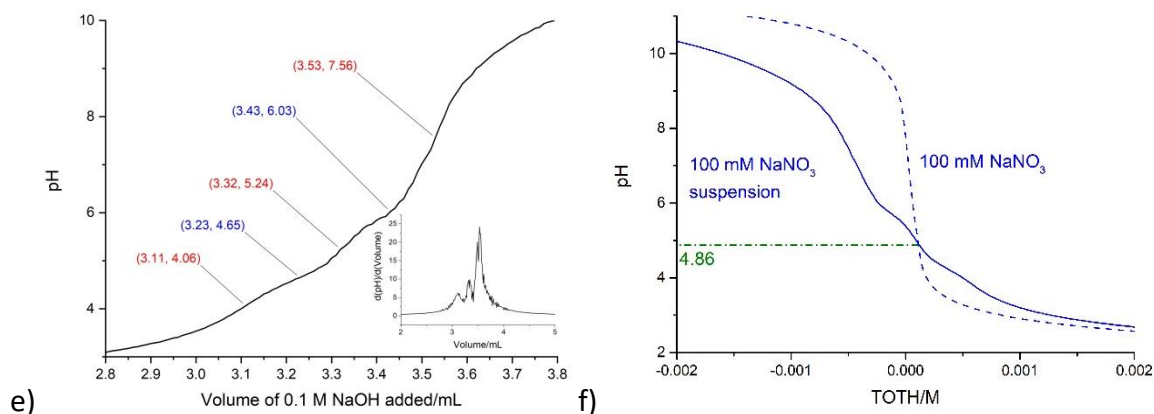


Figure 9: Constant-pH isotherm data for the adsorption of Mg (black) and Ca (green) on acid-washed garnet, with a comparison of different methods of fitting the data, as described in the text. Solids lines indicate fits obtained from numerical modelling using a two-layer model; dashed lines indicate Langmuir-type fits; the red dotted line indicates a Freundlich-type fit for the Ca data. Error bars represent experimental and dilution errors of each sample.

### Acid-Base Titrations

If sodium nitrate is assumed to be an effectively inert electrolyte towards acid-washed garnet powder, then the addition of nitric acid or sodium hydroxide allows the pH of the suspension to be adjusted and the protonation or deprotonation of the surface groups (Equations 1 and 2) to be monitored, without the possibility of specific adsorption of ions. Figure 10 shows acid-base titration curves in different concentrations of sodium nitrate; a), c), and e) show the 'raw' data, plotting the measured pH against the increasing volume of base added to the (pre-acidified) sample; in b), d), and f) the horizontal axis is converted to the effective concentration of acid added (TOTM), and dotted lines indicating the responses of 'blank' samples (without garnet powder) are also shown.





**Figure 10: a), c), and e) acid-base titration curves for 50 g L<sup>-1</sup> (unless otherwise stated) suspensions of acid-washed almandine garnet in 50 mL of 10 mM, 50 mM (45 g L<sup>-1</sup>), and 100 mM NaNO<sub>3</sub> respectively. Equivalence points are labelled in red, and equilibrium points are labelled in blue. Insets: first derivatives of pH with respect to volume of titrant. b), d), and f) correspond to a), c), and e) respectively and show the variation in pH against TOTH, the concentration found from the difference of the number of moles of acid and base added to the electrolyte, (solid lines) compared to the response of the 'blank' electrolyte only (dotted lines); the intersection of the two curves indicates the pzc of the garnet powder.**

It is evident that the pH change as base is added is much more abrupt for the 'blank' samples than for the samples containing garnet powder. This is entirely consistent with the surface groups of the garnet deprotonating, thereby effectively buffering the solution and slowing the pH rise. It is somewhat surprising that the curves appear almost identical, regardless of the electrolyte concentration: one would expect that at lower electrolyte concentrations, formation of a highly charged surface is less favourable and so the pH change occurs more abruptly (the surface groups tend to remain as  $\equiv \text{XOH}$ , rather than protonating to  $\equiv \text{XOH}_2^+$  or deprotonating to  $\equiv \text{XO}^-$ ). One plausible explanation for this is that no surface charge develops during the titration, because the surface reactions occurring are effectively the pH-dependent specific adsorption of sodium and

nitrate ions (Equations 5 and 9). However, one would also expect the extent of these reactions to be dependent on the concentration of sodium nitrate electrolyte, and so the explanation for this observation remains unclear.

Considering Figure 10 a), c), and e) as simple acid-base titrations (discounting any charging of the surface and specific adsorption of ions), the insets, which show the first derivatives of the titration curves with respect to the volume of base added, highlight the points of highest and lowest gradient, respectively the equivalence points and the acid dissociation constants (the  $pK_a$  values). In agreement with what we have reported previously,<sup>5</sup> the  $pK_a$  values are 4.43 ( $\pm 0.09$ ) and 6.13 ( $\pm 0.06$ ). These values show general agreement to the predictions made earlier for the  $pK_a$  values of the hydroxyl groups that form on the surface, based on the binding energy of the surface oxygen peak observed in XPS from almandine garnet, 3.41 ( $\pm 0.62$ ) and 7.41 ( $\pm 0.96$ ), confirming the validity of the prediction method used.

$pK_a$  values are available in different solvents for a number of surface groups: different elements coordinating to the surface hydroxide affect its acidity/basicity, although different measurement methods may measure different parameters, leading to apparent variation in the  $pK_a$  values.<sup>31</sup> One of the best-studied cases, that of silanol groups on silica surfaces, is complex: there can be a number of differently coordinated groups present,<sup>55</sup> and the  $pK_a$  values range from 4.5 to 9.2.<sup>56–59</sup> Singly coordinated aluminium hydroxide groups, 'Al-OH' are reported to have a  $pK_a$  value of 10 in gibbsite or 7 in kaolinite.<sup>58,60,61</sup> The  $pK_a$  values for iron hydroxide surface groups range from 5 to 9, depending on the type of iron oxide and the preparation of the surface.<sup>12,31</sup> Given the range of literature  $pK_a$  values for surface groups coordinated to silicon, aluminium, and iron, it is not possible to determine the nature of the surface groups on almandine garnet based solely on titration data.

However, these  $pK_a$  values can provide insight into the surface acidity of the mineral. It is noteworthy that two  $pK_a$  values are observed, suggesting that either there is only one type of surface group, which deprotonates twice in sodium nitrate electrolyte in the pH range considered (Equations 1 and 2), or that two distinct surface groups are present, each of which deprotonates once in the pH range. It is also possible to estimate the densities of these surface sites from the titration data, by dividing the number of hydroxide ions (which deprotonate the surface groups) added between the equivalence points by the surface area of the almandine garnet powder in the suspension (using the specific surface area,  $5.54 (\pm 0.03) \text{ m}^2 \text{ g}^{-1}$ ). The site densities are estimated to be  $0.71 (\pm 0.08) \text{ sites nm}^{-2}$ , in reasonable agreement with the  $1.05 (\pm 0.08) \text{ sites nm}^{-2}$  reported previously.<sup>5</sup> The same value is found for both of the deprotonation steps, consistent with either the titrations only identifying one type of surface group (which deprotonates twice), or with there being two surface groups, with the same site densities.

The point of zero charge (pzc) of acid-washed almandine garnet powder can also be extracted from the titration data, by comparing the change in pH (with different amounts of added acid or base) of almandine garnet in sodium nitrate to that of the sodium nitrate only: the pzc is the pH at which the solid and dotted curves in Figure 10b), d), and f) intersect. Considering all different samples and different concentrations of sodium nitrate electrolyte, the pzc is  $4.75 (\pm 0.07)$ . Although this value is slightly lower than the pH of  $4.93 (\pm 0.08)$  observed when acid-washed garnet is added to ultrapure water (as discussed in the Salt-Solution Titrations Section), there does not appear to be any systematic change in the pzc with different concentrations of sodium nitrate (between 10 and 100 mM), which is consistent with the specific adsorption of the sodium and nitrate ions being negligible. Our pzc value is in good agreement with the literature pzc value for almandine garnet in sodium perchlorate solution, 4.5,<sup>52</sup> confirming that the acid washing process does not significantly change the surface.

It is noteworthy that the pzc determined from the acid-base titration, 4.75 ( $\pm$  0.07), differs somewhat from the pzc that would be found by taking the mean of the  $pK_a$  values, 5.28 ( $\pm$  0.05): this would be the pzc if the doubly-protonated (positive) and unprotonated (negative) surface groups are the only charged groups present, and they have the  $pK_a$  values given above. Although the difference is relatively small, it may highlight the limitation of considering these data as simple acid-base titrations: the surface charge and the protonation and deprotonation processes are mutually linked, and so the 'stationary' points in the titration curves do not accurately give surface  $pK_a$  values, as they would if the change in surface charge (and the specific adsorption of ions) could be neglected.

There are significant numbers of literature experimental and theoretical studies of different surfaces' pzc and isoelectric points (iep).<sup>52,62,41</sup> Pzc values are typically determined by potentiometric titration, whereas iep values are usually measured electrokinetically, for example by  $\zeta$ -potential measurements,<sup>63</sup> although in an effectively inert electrolyte, the pzc and iep values coincide.<sup>64</sup>  $\zeta$ -potential measurements for acid-washed garnet powders will be discussed subsequently. Silica surfaces with silanol surface groups have pzc values ranging from 1.6 for quartz to 3.4 for vitreous silica.<sup>65</sup> By contrast, aluminum oxide has a pzc of 8,<sup>66</sup> and gibbsite,  $\gamma$ -Al(OH)<sub>3</sub>, has a pzc between 9 and 10.<sup>67</sup> The pzc of iron oxides are generally around 8 to 10, although for natural ferrihydrite the value is in the range 5.3 to 7.5.<sup>68</sup> Whilst the similarity of this value to that for acid-washed garnet may suggest that garnet shares similar functionalities to natural ferrihydrites, the range of pzc values seen for silicon, aluminum and iron oxide surfaces make it impossible to conclusively determine the nature of the groups on the garnet surface from the pzc value.

Figure 11 shows acid-base titration curves for acid-washed garnet powder in 100 mM sodium nitrate with 100 mM (a) magnesium nitrate or (b) calcium nitrate; curves for the powder in sodium

nitrate only are shown (in blue) for comparison, as are dotted curves indicating the response of the 'blank' electrolyte only. In the low-pH region, the addition of magnesium or calcium nitrate does not affect the titration curve; this is unsurprising, because adsorption of the cations becomes more significant at higher pH, as was observed in the variable-pH adsorption data. However, as the magnesium or calcium begins to adsorb, displacing protons from the surface, more base must be added to raise the pH than in the case when only sodium nitrate is present. A consequence of this change is that the crossover point (of the curves for the acid-washed garnet and the electrolyte only) shifts to lower pH (to 3.90 and 4.29 respectively) when 100 mM magnesium or calcium nitrate is added. This shift is in line with literature observations on haematite.<sup>69</sup> It is important to recognise that when specific adsorption of ions is significant, the crossover point does not represent the true pzc of the surface: specifically adsorbed cations can make the surface positively charged, even at high pH.

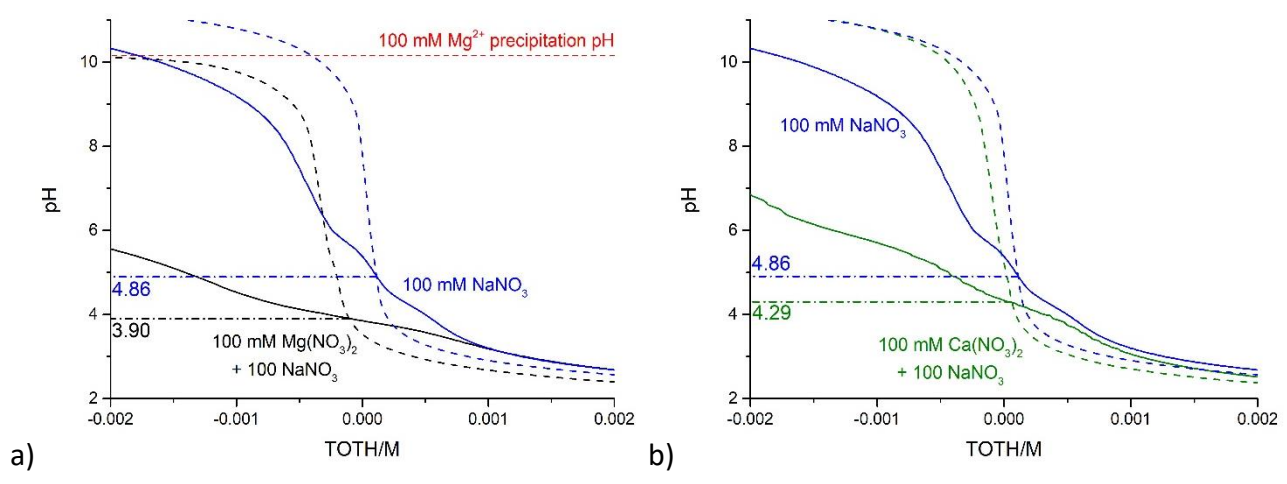


**Figure 11: Acid-base titration curves (plotted as pH against TOTH, the concentration found from the difference of the number of moles of acid and base added to the electrolyte) for 50 g L<sup>-1</sup> suspensions of acid-washed almandine garnet (solid lines) in 50 mL of 100 mM NaNO<sub>3</sub> (blue), and with 100 mM a) Mg(NO<sub>3</sub>)<sub>2</sub> (black) or b) Ca(NO<sub>3</sub>)<sub>2</sub> (green) added; dashed lines indicate the response of the 'blank' electrolyte (without garnet powder) only.**

## Zeta- ( $\zeta$ -) Potential Measurements

$\zeta$ -Potential measurements, which involve measuring the potential at the slip-plane, can be useful in determining the nature of surface groups and specifically adsorbed ions, and the immobilised species present in the diffuse layer, at different pH.<sup>70</sup> Figure 12 shows the measured  $\zeta$ -potential of acid-washed garnet particles suspended in different concentrations of a) sodium nitrate and b) sodium chloride at varying pH. Similar behaviour is seen for the two electrolytes, with positive and negative  $\zeta$ -potentials observed at low and high pH respectively. This is consistent with what would be expected in an inert electrolyte: the  $\zeta$ -potential is positive at pH below the pristine pzc and negative at higher pH, as a consequence of the dominant surface groups being  $\equiv \text{XOH}_2^+$  and  $\equiv \text{XO}^-$ , or similar, at low and high pH respectively.

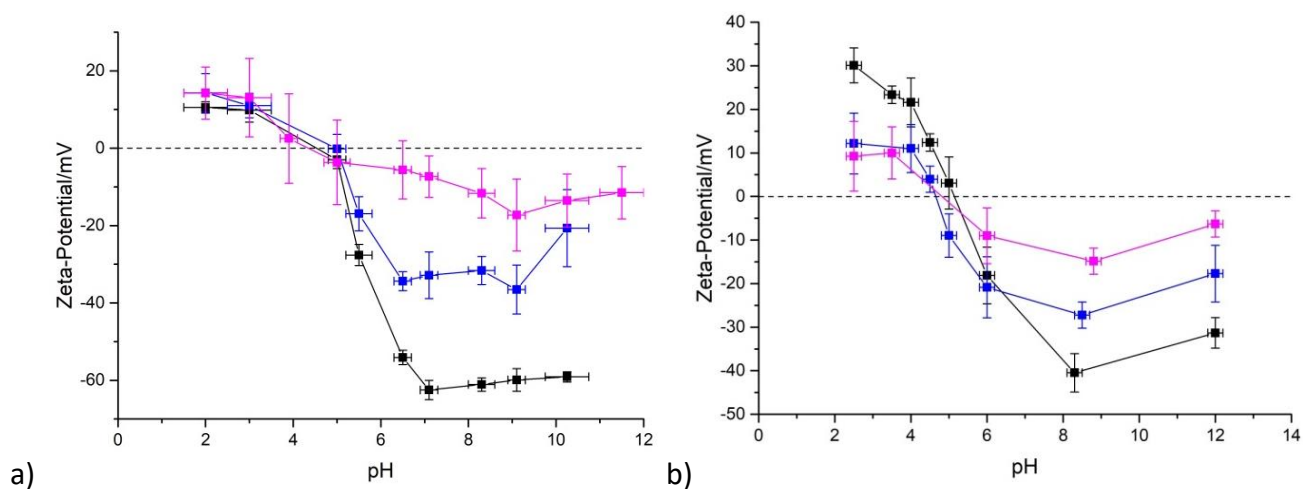


**Figure 12:  $\zeta$ -Potential measurements for 1 g L<sup>-1</sup> suspensions of acid-washed garnet powder in 10 mM (black), 100 mM (blue), or 1 M (magenta) a) NaNO<sub>3</sub> or b) NaCl.  $\zeta$ -Potential error bars indicate the standard deviation of repeated measurements; pH error bars represent the uncertainty of the high-precision pH paper used to measure suspension pH.**

The pH at which the  $\zeta$ -potential is zero (the iep) shows no systematic dependence on the electrolyte concentration in either case, taking values of 4.6 ( $\pm$  0.4) and 4.9 ( $\pm$  0.3) for sodium

nitrate and sodium chloride respectively. The good agreement between the iep ( $4.6 (\pm 0.4)$ ), the pzc determined from acid-base titrations in sodium nitrate ( $4.75 (\pm 0.07)$ ), and the literature value of the pzc in sodium perchlorate solution ( $4.5$ )<sup>52</sup> is again consistent with sodium nitrate being an effectively inert electrolyte towards the garnet surface. Furthermore, the similarity between the  $\zeta$ -potential data in sodium nitrate and sodium chloride suggests that the behaviour of the chloride and nitrate ions is similar, and that neither adsorbs specifically on the surface to a significant extent. Away from the iep, the magnitude of the  $\zeta$ -potential decreases at higher ionic strength, due to increased charge screening by the electrolyte; this is not indicative of a decrease in the magnitude of the surface charge.

Specific adsorption of cations or anions, or their inclusion in the diffuse layer, can lead to the  $\zeta$ -potential being more positive or negative respectively. The measured  $\zeta$ -potentials at varying pH of acid-washed almandine garnet powder in 100 mM sodium nitrate with 100 mM of calcium nitrate, magnesium nitrate, or sodium sulphate are shown in Figure 13. With magnesium or calcium nitrate added, the trend in the  $\zeta$ -potential at low pH is similar to that observed in 100 mM sodium nitrate only (the blue data in Figure 12 a)), but at higher pH, the  $\zeta$ -potential is positive, whereas in sodium nitrate only it is negative. This behaviour is entirely consistent with what might be expected from variable-pH adsorption data (Figure 6): at low pH, the divalent cations do not adsorb on the garnet surface, and so the sign of the  $\zeta$ -potential is unchanged; at higher pH, specific adsorption of magnesium or calcium becomes significant, resulting in positively charged surface groups (of the form of  $\equiv \text{XOMg}^+$ , or similar), and so the  $\zeta$ -potential is positive.

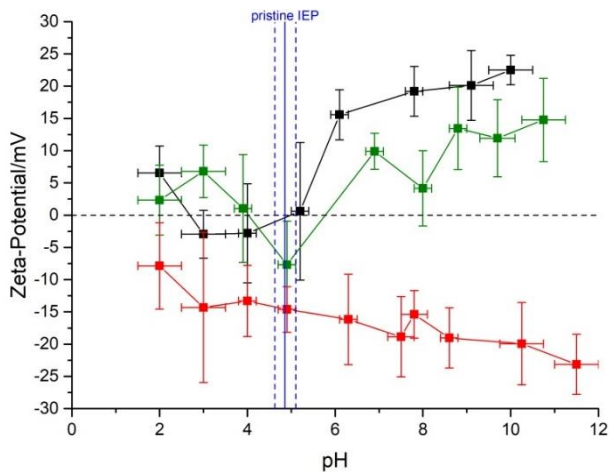


**Figure 13:**  $\zeta$ -Potential measurements for  $1 \text{ g L}^{-1}$  suspensions of acid-washed almandine garnet powder in  $100 \text{ mM NaNO}_3$  with  $100 \text{ mM Mg(NO}_3)_2$  (black),  $\text{Ca(NO}_3)_2$  (green), or  $\text{Na}_2\text{SO}_4$  (red) at different pH. The solid blue line indicates the ‘pristine’ pzc of garnet, with the dotted lines indicating its range within one standard deviation.  $\zeta$ -Potential error bars indicate the standard deviation of repeated measurements; pH error bars show the uncertainty of the pH paper used.

By contrast, when sodium sulphate is added, the  $\zeta$ -potential is negative at high pH, but remains negative at low pH. This behaviour is consistent with the sulphate ions adsorbing at low pH, resulting in negatively charged surface groups (of the form of  $\equiv \text{XSO}_4^-$ , or similar). We have observed some evidence of the adsorption of sulphate ions at low pH in variable-pH isotherms, which supports this interpretation of the  $\zeta$ -potential data; however, given the possibility of dissolution of the almandine garnet powder at these low pH values, the specific adsorption of sulphate ions on the surface remains uncertain.

## Conclusions

In this work, we have used a range of range of experimental techniques and numerical modelling to characterise the surface of almandine garnet, a mineral whose surface chemistry is significant due to its use in abrasive blasting, which results in it being present on ‘clean’ steel surfaces prior to the

application of protective paint layers. We have considered both the 'dry' garnet surface and the response of garnet powders to aqueous solutions of varying pH containing different inorganic ions: this is relevant to remedial work on structures in marine environments, where aerosol droplets are expected to impact the surface in the time between abrasive blasting and repainting, depositing inorganic ions.

XPS data from a polished almandine garnet crystal have indicated that under-coordinated aluminium, silicon, and oxygen atoms all exist in a surface region that is of the order of 0.9 nm thick. Although the precise chemical nature of the surface hydroxyl groups that will form on hydration of this surface is difficult to predict, we have suggested a novel method of doing this using the correlation between the  $pK_a$  values of surface hydroxyl groups that form on several elemental oxides and the binding energies of their oxygen 1s XPS surface peaks; this has allowed us to predict  $pK_a$  values, based on the almandine garnet ARXPS data, that are in general agreement with the values obtained from acid-base titrations of garnet powder.

From salt-solution and acid-base titrations, adsorption isotherm data, and  $\zeta$ -potential measurements, it is clear that the divalent magnesium and calcium cations adsorb specifically on the almandine garnet surface. Adsorption becomes more significant at high pH; at pH 9.35, Langmuir-type fits show good agreement to the experimental data, with plateau adsorption at around 1.4 and 2.1 cations  $\text{nm}^{-2}$  for magnesium and calcium respectively. The adsorption of calcium is evidently somewhat stronger than that of magnesium, whilst there is also some evidence that there are different adsorption mechanisms for the two cations and that calcium adsorbs on two distinct types of surface site. No evidence of specific adsorption of the monovalent nitrate and chloride anions has been seen at any pH, but  $\zeta$ -potential measurements suggest that the divalent sulphate anion may adsorb at low pH, although garnet powder tends to dissolve in strong acid.

The behaviour of the monovalent sodium cation is somewhat unclear: salt-solution titrations suggest weak adsorption to the surface, and simple numerical modelling provides best fits to the adsorption isotherm data (for magnesium and calcium) with a high surface-site density ( $40 \text{ nm}^{-2}$ ) and competition between the weakly-binding sodium and the more-strongly-binding divalent cations; however, acid-base titrations and  $\zeta$ -potential measurements suggest that sodium is effectively inert towards specific adsorption on the surface, with a small number of surface sites ( $0.7 \text{ nm}^{-2}$ ) becoming doubly protonated at low pH and unprotonated at high pH in sodium nitrate, resulting in a positively or negatively charged surface respectively. The point of zero charge of garnet powder in sodium nitrate solutions of different ionic strength, approximately 4.75, is in good agreement with literature values of the point of zero charge of almandine garnet in sodium chlorate solution, 4.5, further suggesting that sodium nitrate is effectively an inert electrolyte towards the garnet surface at the concentrations tested.

We have successfully fitted salt-solution titration and cation-adsorption data using a simple two-layer numerical model with one type of almandine garnet surface site. However, the range of experimental data we have compiled in this work has emphasized that one must exercise caution when attempting to interpret different data using a single model: For almandine garnet, a mineral containing (at least) four different atoms in its bulk structure, it is most probable that the exposed surface is rather heterogeneous, with a number of different surface groups present; the protonation and deprotonation of these, their ability to specifically adsorb ions, and the resulting changes in surface charge and the composition of the diffuse layer are all crucial factors in determining the response of the surface when it is in contact with aqueous solution. The complex behaviour observed in this work highlights the difficulty in separating these contributing factors, as would be needed to make general predictions about the behaviour of similar surfaces in different conditions.

## **Acknowledgments**

The authors thank the Royal Dutch Shell for their funding and technical support, in particular Dr Lene Hviid and Dr Damodaran Raghu. The authors also thank Dr Chris Truscott at the Department of Chemistry, University of Cambridge for his assistance with PXRD data collection and analysis, Stephen Young at the Department of Chemistry and Dr Chris Rolfe at the Department of Geography, University of Cambridge for their assistance in ICP-OES analysis, and Dr Robert Palgrave at University College London (part of the Harwell XPS Service) and Chris Amey at the Cavendish Laboratory, University of Cambridge for their assistance in XPS data collection. The XPS data collection at the EPSRC National Research Facility HarwellXPS was performed under contract number PR16195.

## **Supporting Information Available**

Table S1 shows the quoted composition of the almandine garnet ('garnet') abrasive; Figure S1 shows a unit cell of the almandine garnet crystal structure in polyhedral representation; Figure S2 reports powder X-ray diffraction data of almandine garnet before and after acid washing, with powders tumbled for one week in 0.1 M HCl, ultrapure water, or 0.1 M NaOH; Figure S3 reports AR-XP spectra for the Fe 2p region at 0° and 50° surveying angles, and the corresponding peak fitting results; Figure S4 reports the surface layer thicknesses calculated from AR-XP spectra at different surveying angles for Al, Si, and O; Table S2 reports ICP-OES results indicating the dissolved Fe, Al, and Si after tumbling acid-washed garnet powder in 0.1 M HCl, ultrapure water, or 0.1 M NaOH for one week; Figure S5 reports the different site densities used to fit the experimental salt-solution titration data with numerical modelling and the equilibrium constant that provides the best fit in each case. This material is available free of charge via the Internet at <http://pubs.acs.org>.

## References

- (1) Novak, G. A.; Gibbs, G. V. The Crystal Chemistry of the Silicate Garnet. *Am. Mineral.* **1971**, *56*, 791–825.
- (2) Stewart, H. A. Stock Removal Rates For Aluminium Oxide-Coated and Garnet-Coated Abrasive Belts. *For. Prod. Journal.* **1978**, *28* (11), 29–31.
- (3) Olson, D. W. *Mineral Commodity Summaries*; United States Department of the Interior: Washington D. C., 2005.
- (4) Harben, H. W.; Kužvart, M. *Industrial Minerals: A Global Geology*, 1st ed.; Industrial Minerals Information Ltd.: London, UK, 1996.
- (5) Poon, J.; Madden, D. C.; Wood, M. H.; Clarke, S. M. Characterizing Surfaces of Garnet and Steel, and Adsorption of Organic Additives. *Langmuir* **2018**, *34* (26), 7726–7737.
- (6) Hansley, P. L.; Briggs, P. H. *Garnet Dissolution in Oxalic Acid - a Possible Analog for Natural Etching of Garnet by Dissolved Organic Matter*; Denver, USA, 1994.
- (7) Grandstaff, D. E. Changes in Surface Area and Morphology and the Mechanism of Forsterite Dissolution. *Geochim. Cosmochim. Acta* **1978**, *42* (12), 1899–1901.
- (8) Jia, M.-X.; Sun, C.-Y. Flotation and Surface Characteristics of Some Silicate Minerals and Its Crystal Chemistry Analysis. *Conserv. Util. Miner. Resour.* **2001**, *5*, 25–29.
- (9) Jia, M.-X.; Sun, C.-Y. Study of Adsorption Behaviour of Metal Ions On Some Silicate Minerals. *Min. Metall.* **2001**, *10* (3), 25–30.
- (10) Poon, J.; Collins, S. M.; Madden, D. C.; Sonke, H.; Clarke, S. M. Characterization of Short Time Marine Corroded Surfaces. *J. Electrochem. Soc.* **2019**, *166* (14), C509–C519.

- (11) Koretsky, C. M.; Sverjensky, D. A.; Salisbury, J. W.; D'Aria, D. M. Detection of Surface Hydroxyl Species on Quartz,  $\gamma$ -Alumina, and Feldspars Using Diffuse Reflectance Infrared Spectroscopy. *Geochim. Cosmochim. Acta* **1997**, *61* (11), 2193–2210.
- (12) Dzombak, D. A.; Morel, F. M. M. *Surface Complexation Modeling: Hydrous Ferric Oxide*, 1st ed.; John Wiley & Sons, Inc., 1990.
- (13) Hsiao, Y.-H.; La Plante, E. C.; Krishnan, N. M. A.; Dobbs, H. A.; Le Pape, Y.; Neithalath, N.; Bauchy, M.; Israelachvili, J.; Sant, G. Role of Electrochemical Surface Potential and Irradiation on Garnet-Type Almandine's Dissolution Kinetics. *J. Phys. Chem. C* **2018**, *122* (30), 17268–17277.
- (14) Matsumoto, R.; Nishizawa, Y.; Kataoka, N.; Tanaka, H.; Yoshikawa, H.; Tanuma, S.; Yoshihara, K. Reproducibility of XPS Analysis for Film Thickness of SiO<sub>2</sub>/Si by Active Shirley Method. *J. Electron Spectros. Relat. Phenomena* **2016**, *207*, 55–59.
- (15) Tougaard, S.; Jansson, C. Background Correction in XPS: Comparison of Validity of Different Methods. *Surf. Interface Anal.* **1992**, *19* (1–12), 171–174.
- (16) McCafferty, E.; Wightman, J. P. Determination of the Concentration of Surface Hydroxyl Groups on Metal Oxide Films by a Quantitative XPS Method. *Surf. Interface Anal.* **1998**, *26* (8), 549–564.
- (17) Simmons, G. W.; Beard, B. C. Characterization of Acid-Base Properties of the Hydrated Oxides on Iron and Titanium Metal Surfaces. *J. Phys. Chem.* **1987**, *91* (5), 1143–1148.
- (18) Nesbitt, H. W.; Banerjee, D. Interpretation of XPS Mn(2p) Spectra of Mn Oxyhydroxides and Constraints on the Mechanism of MnO<sub>2</sub> Precipitation. *Am. Mineral.* **1998**, *83* (3–4), 305–315.
- (19) Langell, M. A.; Hutchings, C. W.; Carson, G. A.; Nassir, M. H. High Resolution Electron Energy

- Loss Spectroscopy of MnO(100) and Oxidized MnO(100). *J. Vac. Sci. Technol. A Vacuum, Surfaces, Film.* **1996**, *14* (3), 1656–1661.
- (20) Junta, J. L.; Hochella, M. F. Manganese (II) Oxidation at Mineral Surfaces: A Microscopic and Spectroscopic Study. *Geochim. Cosmochim. Acta* **1994**, *58* (22), 4985–4999.
- (21) Zaki, M. I.; Hasan, M. A.; Pasupulety, L.; Kumari, K. Bulk and Surface Characteristics of Pure and Alkalized Mn<sub>2</sub>O<sub>3</sub>: TG, IR, XRD, XPS, Specific Adsorption and Redox Catalytic Studies. *New J. Chem.* **1998**, *22* (8), 875–882.
- (22) Ohashi, H.; Ezo, H.; Okaue, Y.; Kobayashi, Y.; Matsuo, S.; Kurisaki, T.; Miyazaki, A.; Wakita, H.; Yokoyama, T. The Effect of UV Irradiation on the Reduction of Au(III) Ions Adsorbed on Manganese Dioxide. *Anal. Sci.* **2005**, *21* (7), 789–793.
- (23) Judd, R. W.; Komodromos, C.; Reynolds, T. J. Alkali Chloride Doped Manganese Oxide Catalysts: Nature of the Active Surface. *Catal. Today* **1992**, *13* (2–3), 237–244.
- (24) Hernandez Ubeda, M.; Mishima, H. T.; López de Mishima, B. A. The Electrochemical Response of Manganese Hydroxide-Oxide Films in Slightly Alkaline Solutions-I. The Redox Couple. *Electrochim. Acta* **1991**, *36* (5–6), 1013–1018.
- (25) Mustafa, S.; Zaman, M. I.; Khan, S. PH Effect on Phosphate Sorption by Crystalline MnO<sub>2</sub>. *J. Colloid Interface Sci.* **2006**, *301* (2), 370–375.
- (26) Portehault, D.; Cassaignon, S.; Baudrin, E.; Jolivet, J.-P. Selective Heterogeneous Oriented Attachment of Manganese Oxide Nanorods in Water: Toward 3D Nanoarchitectures. *J. Mater. Chem.* **2009**, *19* (42), 7947–7954.
- (27) Yamashita, T.; Hayes, P. Analysis of XPS Spectra of Fe<sup>2+</sup> and Fe<sup>3+</sup> Ions in Oxide Materials. *Appl. Surf. Sci.* **2008**, *254* (8), 2441–2449.

- (28) McIntyre, N. S.; Zetaruk, D. G. X-Ray Photoelectron Spectroscopic Studies of Iron Oxides. *Anal. Chem.* **1977**, *49* (11), 1521–1529.
- (29) Scheidegger, A.; Borkovec, M.; Sticher, H. Coating of Silica Sand with Goethite: Preparation and Analytical Identification. *Geoderma* **1993**, *58* (1–2), 43–65.
- (30) Allen, G. C.; Curtis, M. T.; Hooper, A. J.; Tucker, P. M. X-Ray Photoelectron Spectroscopy of Iron-Oxygen Systems. *J. Chem. Soc. Dalton Trans.* **1974**, *0* (14), 1525–1530.
- (31) Cornell, R. M.; Schwertmann, U. *Surface Chemistry and Colloidal Stability*, 2nd ed.; Wiley-VCH Verlag GmbH & Co. KGaA: Weinheim, Germany, 2003.
- (32) McCafferty, E.; Wightman, J. P.; Cromer, T. F. Surface Properties of Hydroxyl Groups in the Air-Formed Oxide Film on Titanium. *J. Electrochem. Soc.* **1999**, *146* (8), 2849.
- (33) Sham, T. K.; Lazarus, M. S. X-Ray Photoelectron Spectroscopy (XPS) Studies of Clean and Hydrated TiO<sub>2</sub> (Rutile) Surfaces. *Chem. Phys. Lett.* **1979**, *68* (2–3), 426–432.
- (34) Healy, K. E.; Ducheyne, P. Hydration and Preferential Molecular Adsorption on Titanium in Vitro. *Biomaterials* **1992**, *13* (8), 553–561.
- (35) Vörös, J.; Wieland, M.; Ruiz-Taylor, L.; Textor, M.; Brunette, D. M. *Characterization of Titanium Surfaces*, 1st ed.; Brunette, D. M., Tengvall, P., Textor, M., Thomsen, P., Eds.; Springer-Verlag Berlin Heidelberg: Heidelberg, Germany, 2001.
- (36) Cheng, J.; Sprik, M. Acidity of the Aqueous Rutile TiO<sub>2</sub> (110) Surface from Density Functional Theory Based Molecular Dynamics. *J. Chem. Theory Comput.* **2010**, *6* (3), 880–889.
- (37) Bourikas, K.; Kordulis, C.; Lycourghiotis, A. Titanium Dioxide (Anatase and Rutile): Surface Chemistry, Liquid-Solid Interface Chemistry, and Scientific Synthesis of Supported Catalysts.

*Chem. Rev.* **2014**, *114* (19), 9754–9823.

- (38) Strohmeier, B. R. An ESCA Method for Determining the Oxide Thickness on Aluminum Alloys. *Surf. Interface Anal.* **1990**, *15* (1), 51–56.
- (39) Olefjord, I.; Nylund, A. Surface Analysis of Oxidized Aluminium. 2. Oxidation of Aluminium in Dry and Humid Atmosphere Studied by ESCA, SEM, SAM and EDX. *Surf. Interface Anal.* **1994**, *21* (5), 290–297.
- (40) Iatsunskiy, I.; Kempniński, M.; Jancelewicz, M.; Załęski, K.; Jurga, S.; Smyntyna, V. Structural and XPS Characterization of ALD Al<sub>2</sub>O<sub>3</sub> Coated Porous Silicon. *Vacuum* **2015**, *113*, 52–58.
- (41) Hiemstra, T.; Venema, P.; Riemsdijk, W. H. V. Intrinsic Proton Affinity of Reactive Surface Groups of Metal (Hydr)Oxides: The Bond Valence Principle. *J. Colloid Interface Sci.* **1996**, *184* (2), 680–692.
- (42) Franks, G. V.; Gan, Y. Charging Behavior at the Alumina–Water Interface and Implications for Ceramic Processing. *J. Am. Ceram. Soc.* **2007**, *90* (11), 3373–3388.
- (43) Schaefer, J. A.; Anderson, J.; Lapeyre, G. J. Water Adsorption on Cleaved Silicon Surfaces. *J. Vac. Sci. Technol. A Vacuum, Surfaces, Film.* **1985**, *3* (3), 1443–1447.
- (44) Duval, Y.; Mielczarski, J. A.; Pokrovsky, O. S.; Mielczarski, E.; Ehrhardt, J. J. Evidence of the Existence of Three Types of Species at the Quartz–Aqueous Solution Interface at PH 0–10: XPS Surface Group Quantification and Surface Complexation Modeling. *J. Phys. Chem. B* **2002**, *106* (11), 2937–2945.
- (45) Simmons, G. W.; Angst, D. L.; Klier, K. A Self-Modeling Approach to the Resolution of XPS Spectra into Surface and Bulk Components. *J. Electron Spectros. Relat. Phenomena* **1999**, *105* (2–3), 197–210.

- (46) Scales, P. J.; Grieser, F.; Healy, T. W.; White, L. R.; Chan, D. Y. C. Electrokinetics of the Silica-Solution Interface: A Flat Plate Streaming Potential Study. *Langmuir* **1992**, *8* (3), 965–974.
- (47) Ong, S.; Zhao, X.; Eisenthal, K. B. Polarization of Water Molecules at a Charged Interface: Second Harmonic Studies of the Silica/Water Interface. *Chem. Phys. Lett.* **1992**, *191* (3–4), 327–335.
- (48) Allen, L. H.; Matijević, E.; Meites, L. Exchange of Na<sup>+</sup> for the Silanolic Protons of Silica. *J. Inorg. Nucl. Chem.* **1971**, *33* (5), 1293–1299.
- (49) Koretsky, C. The Significance of Surface Complexation Reactions in Hydrologic Systems: A Geochemist's Perspective. *J. Hydrol.* **2000**, *230* (3–4), 127–171.
- (50) Velbel, M. A. Natural Weathering Mechanisms of Almandine Garnet. *Geology* **1984**, *12* (10), 631.
- (51) Modi, H. J.; Fuerstenau, D. W. Streaming Potential Studies on Corundum in Aqueous Solutions of Inorganic Electrolytes. *J. Phys. Chem.* **1957**, *61* (5), 640–643.
- (52) Kosmulski, M. *Surface Charging and Points of Zero Charge*; CRC Press: Boca Raton, USA, 2009.
- (53) Brown, P. L.; Ekberg, C. *Hydrolysis of Metal Ions*, 1st ed.; Wiley-VCH Verlag GmbH & Co. KGaA: Weinheim, Germany, 2016.
- (54) Iler, R. K. *The Chemistry of Silica : Solubility, Polymerization, Colloid and Surface Properties, and Biochemistry*, 1st ed.; John Wiley & Sons, Inc.: Hoboken, USA, 1979.
- (55) Hsu, W. L.; Daiguji, H.; Dunstan, D. E.; Davidson, M. R.; Harvie, D. J. E. Electrokinetics of the Silica and Aqueous Electrolyte Solution Interface: Viscoelectric Effects. *Adv. Colloid Interface*

*Sci.* **2016**, *234*, 108–131.

- (56) Filho, N. L. D.; do Carmo, D. R. *Encyclopedia of Surface and Colloid Science, Adsorption at Silica, Alumina, and Related Surfaces*, 1st ed.; Somasundaran, P., Ed.; Marcel Dekker, Inc.: New York, USA, 2004.
- (57) Leung, K.; Nielsen, I. M. B.; Criscenti, L. J. Elucidating Acid-Base Behavior of Silica with Ab Initio Molecular Dynamics. *Nanosci. Nanotechnol.* **1992**, No. 505, 56–57.
- (58) Hair, M. L.; Hertl, W. Acidity of Surface Hydroxyl Groups. *J. Phys. Chem.* **1970**, *74* (1), 91–94.
- (59) Leung, K.; Nielsen, I. M. B.; Criscenti, L. J. Elucidating the Bimodal Acid-Base Behavior of the Water-Silica Interface from First Principles. *J. Am. Chem. Soc.* **2009**, *131* (51), 18358–18365.
- (60) Rosenqvist, J. *Surface Chemistry of Al and Si (Hydr)Oxides, with Emphasis on Nano-Sized Gibbsite ( $\alpha$ -Al (OH)<sub>3</sub>)*, Umea University, 2002.
- (61) Karamalidis, A. K.; Dzombak, D. A. Surface Properties of Gibbsite. In *Surface Complexation Modeling: Gibbsite*; John Wiley & Sons, Inc.: Hoboken, USA, 2010; pp 59–80.
- (62) Kosmulski, M. The PH Dependent Surface Charging and Points of Zero Charge. VI. Update. *J. Colloid Interface Sci.* **2014**, *426*, 209–212.
- (63) Drzymala, J.; Sadowski, Z.; Holysz, L.; Chibowski, E. Ice/Water Interface: Zeta Potential, Point of Zero Charge, and Hydrophobicity. *J. Colloid Interface Sci.* **1999**, *220* (2), 229–234.
- (64) Kosmulski, M. The PH-Dependent Surface Charging and Points of Zero Charge: V. Update. *J. Colloid Interface Sci.* **2011**, *353* (1), 1–15.
- (65) Persello, J. *Adsorption on Silica Surfaces*, 1st ed.; Papirer, E., Ed.; Marcek Dekker, Inc.: New York, USA, 2000.

- (66) Tombácz, E. PH-Dependent Surface Charging of Metal Oxides. *Period. Polytech. Chem. Eng.* **2009**, *532*, 77–86.
- (67) Adekola, F.; Fédoroff, M.; Geckeis, H.; Kupcik, T.; Lefèvre, G.; Lützenkirchen, J.; Plaschke, M.; Preocanin, T.; Rabung, T.; Schild, D. Characterization of Acid–Base Properties of Two Gibbsite Samples in the Context of Literature Results. *J. Colloid Interface Sci.* **2011**, *354* (1), 306–317.
- (68) *Environmental Impact of Soil Component Interactions: Metals, Other Inorganics, and Microbial Activities. Volume II*, 1st ed.; Huang, P. M., Berthelin, J., Bollag, J.-M., McGill, W. B., Page, A. L., Eds.; Lewis Publishers: Boca Raton, USA, 1995.
- (69) Ardizzone, S.; Formaro, L.; Lyklema, J. Adsorption from Mixtures Containing Mono- and Bivalent Cations on Insoluble Oxides and a Revision of the Interpretation of Points of Zero Charge Obtained by Titration. *J. Electroanal. Chem.* **1982**, *133* (1), 147–156.
- (70) Lyklema, J. *Fundamentals of Interface and Colloid Science. Volume II, Solid-Liquid Interfaces*, 1st ed.; Academic Press: London, UK, 1995.

## TOC Graphic

